

1 **Diurnal Variation in the Coupling of Photosynthetic**
2 **Electron Transport and Carbon Fixation in iron-limited**
3 **Phytoplankton in the NE subarctic Pacific**

4

5 **N. Schuback¹, M. Flecken², M. T. Maldonado¹, P. D. Tortell^{1,3}**

6 [1]{Departement of Earth, Ocean and Atmospheric Sciences, University of British Columbia,
7 Vancouver, BC, Canada}

8 [2]{RWTH Aachen University, Aachen, Germany}

9 [3]{Department of Botany, University of British Columbia, Vancouver, BC, Canada}

10 Correspondence to: N. Schuback (nschuback@eos.ubc.ca)

11

12 **Abstract**

13 Active chlorophyll *a* fluorescence approaches, including fast repetition rate fluorometry
14 (FRRF), have the potential to provide estimates of phytoplankton primary productivity at
15 unprecedented spatial and temporal resolution. FRRF-derived productivity rates are based on
16 estimates of charge separation at PSII (ETR_{RCII}), which must be converted into ecologically
17 relevant units of carbon fixation. Understanding sources of variability in the coupling of ETR_{RCII}
18 and carbon fixation provides physiological insight into phytoplankton photosynthesis, and is
19 critical for the application of FRRF as a primary productivity measurement tool. In the present
20 study, we simultaneously measured phytoplankton carbon fixation and ETR_{RCII} in the iron-
21 limited NE subarctic Pacific, over the course of a diurnal cycle. We show that rates of ETR_{RCII}
22 are closely tied to the diurnal cycle in light availability, whereas rates of carbon fixation appear
23 to be influenced by endogenous changes in metabolic energy allocation under iron-limited
24 conditions. Unsynchronized diurnal oscillations of the two rates led to 3.5-fold changes in the
25 conversion factor coupling ETR_{RCII} and carbon fixation (K_c/nPSII). Consequently, diurnal

26 variability in phytoplankton carbon fixation cannot be adequately captured with FRRF
27 approaches if a constant conversion factor is applied. Utilizing several auxiliary
28 photophysiological measurements, we observed that a high conversion factor is associated with
29 conditions of excess light, and correlates with the increased expression of non-photochemical
30 quenching (NPQ) in the pigment antenna, as derived from FRRF measurements. The observed
31 correlation between NPQ and K_c/n_{PSII} , which requires further validation, has the potential to
32 improve estimates of phytoplankton carbon fixation rates from FRRF measurements alone.

33 **1 Introduction**

34 Marine phytoplankton account for ~ 50% of global carbon fixation (Field et al., 1998), and
35 play a key role in Earth's biogeochemical cycles. Understanding the spatial and temporal patterns
36 in marine primary productivity and its response to environmental variability is thus a central
37 oceanographic research question. Traditionally, rates of phytoplankton primary production have
38 been measured using incubation-based assays, tracing the evolution of oxygen or the assimilation
39 of CO_2 (Williams et al., 2008). Over the past two decades, bio-optical approaches based on
40 measurements of active chlorophyll *a* fluorescence (ChlF) yields (Kolber and Falkowski, 1993;
41 Schreiber, 2004) have emerged as an attractive alternative, avoiding artifacts related to bottle
42 containment, and achieving unparalleled spatial and temporal resolution. The method most
43 prominently applied to measure ChlF yields in field assemblages of marine phytoplankton is fast
44 repetition rate fluorometry (FRRF) (Kolber et al., 1998). ChlF yields, as measured by FRRF, can
45 be used to estimate electron transport in photosystem II (ETR_{RCII} , mol e^- mol $RCII^{-1} s^{-1}$), and
46 these rates can be converted to carbon units based on theoretical calculations. However,
47 empirical comparison of FRRF-derived ETR_{RCII} and carbon fixation data has shown that the
48 derived conversion factor varies significantly with changes in the physiology and taxonomic
49 composition of phytoplankton assemblages (Suggett et al., 2010; Lawrenz et al., 2013).

50 The conversion factor linking ETR_{RCII} and carbon fixation consists of two parameters, the
51 amount of chlorophyll *a* per number of functional PSII reaction centers ($1/n_{PSII}$; mol chl *a* mol
52 $RCII^{-1}$) and the electron requirement for carbon fixation (K_c ; mol e^- mol C^{-1} ; note that in most
53 previous studies, this latter parameter has been denoted as $\Phi_{e:C}$). Plasticity in both $1/n_{PSII}$ and K_c

54 can be observed at the physiological and taxonomic level, and is ultimately a function of given
55 environmental conditions.

56 In order to optimize growth under fluctuating environmental conditions, phytoplankton
57 photosynthesis and downstream metabolic processes exhibit great plasticity and
58 interconnectivity, allowing rapid responds to changes in fluctuating light and nutrient levels. This
59 physiological regulation influences the coupling between ETR_{RCII} and carbon fixation. For
60 example, energy (ATP) and reducing power (NADPH) from the photosynthetic light reaction can
61 be used directly for the reduction or assimilation of limiting nutrients, rather than for carbon
62 fixation (e.g. Laws, 1991; Myers, 1980), resulting in an increased conversion factor $K_c/nPSII$ (e.g.
63 Napoléon et al., 2013). Furthermore, $K_c/nPSII$ has been shown to increase under excess light
64 conditions (Babin et al., 1996; Cheah et al., 2011; Corno et al., 2006; Fujiki et al., 2007; Goto et
65 al., 2008; Kaiblinger and Dokulil, 2006; Napoléon et al., 2013; Napoléon and Claquin, 2012;
66 Raateoja, 2004), when the rate of charge separation in RCII can outpace the rate of electron
67 transport along the photosynthetic electron transport chain (ETC). In order to alleviate the
68 ensuing “backpressure”, which can lead to e.g. singlet oxygen formation and photoinhibition,
69 photosynthetic organisms evolved a number of “safety valves” along the ETC (e.g. Niyogi,
70 2000). Activation of these alternative electron pathways increases the conversion factor $K_c/nPSII$.
71 In a previous study, we showed that low iron concentrations enhanced the effect of excess light,
72 further increasing the conversion factor $K_c/nPSII$ (Schuback et al., 2015).

73 Given the well-established effect of excess light on the coupling of photosynthetic electron
74 transport and carbon fixation, it is likely that the two rates decouple over the course of a diurnal
75 cycle, if excess irradiance is encountered at noon. However, to our knowledge, there are no
76 direct experimental studies of the diurnal changes in the coupling of ETR_{RCII} and carbon fixation
77 in marine phytoplankton.

78 In the present study we simultaneously measured rates of ^{14}C -uptake and ETR_{RCII} in iron-
79 limited phytoplankton assemblages in the NE subarctic Pacific over the course of a 24 hour
80 diurnal cycle. Our results show that the conversion factor $K_c/nPSII$, derived for in situ irradiances
81 at 5 m depth, varied significantly (by a factor of 3.4), with most of the variability attributable to
82 diurnal changes in K_c . Unless both carbon fixation and ETR_{RCII} are measured and integrated over
83 a whole diurnal cycle (e.g. Suggett et al., 2006), diurnal variability in $K_c/nPSII$ should be
84 considered, along with phytoplankton taxonomy and nutrient status (Lawrenz et al., 2013), when

85 deriving regional conversion factors between ETR_{RCII} and carbon fixation. Building on
86 previously published results (Schuback et al., 2015), we show that the magnitude and variability
87 of $K_c/nPSII$ can be correlated to FRRF-based measurements of non-photochemical quenching
88 (NPQ_{NSV}).

89 **2 Methods**

90 **2.1 Study site and water-column hydrography**

91 Field sampling was conducted on board the *CCGS John P. Tully* on June 17th/18th 2014. During
92 the sampling period, the research vessel stayed within close proximity (10 km) to Ocean Station
93 Papa (OSP), located in iron-limited waters of the NE subarctic Pacific (50 °N, 145 °W)
94 (<https://www.waterproperties.ca/linep/>). We acknowledge that our sampling approach is not truly
95 Lagrangian, and some variability in nutritional status and taxonomic composition of
96 phytoplankton assemblage could have occurred due to water mass advection. However, we
97 expect that surface hydrography and phytoplankton characteristics are sufficiently homogeneous
98 in this oceanic region, such that minor water mass advection would not have significantly
99 influenced primary productivity or photophysiological parameters measured over the diurnal
100 cycle.

101 During our occupation of OSP, we conducted five CTD casts (three casts during the 24 hour
102 diurnal experiment and one each before and after the diurnal sampling) to characterize variability
103 in temperature and salinity depth profiles, from which we derived seawater density using the
104 GSW toolbox in MATLAB (McDougall and Barker, 2011). Mixed layer depth (MLD) was
105 calculated from a density difference criterion ($\Delta\sigma = 0.05 \text{ kg m}^{-3}$). The depth profile of
106 photosynthetically available radiation (PAR, 400-700nm, $\mu\text{mol quantum}^{-2} \text{ s}^{-1}$) through the upper
107 100 m of the water column was obtained using a PAR sensor (Biospherical QSP-400) mounted
108 on the rosette during one of the CTD casts (12:30 local time (LT)). The optical extinction
109 coefficient, k_d (m^{-1}), was calculated as:

110
$$k_d = (lnE_0 - lnE_z)/z \quad (1)$$

111 Where E_0 is surface irradiance and E_z is irradiance at depth z (m). Surface PAR (E_0^+) was
112 continuously logged (10 min intervals) with a LI-1000 down-welling PAR sensor (LI-COR,

113 USA), mounted in a non-shaded position on the ship's superstructure, at a height of ca 7 m above
114 the sea-surface. Unfortunately, 3 hours of PAR data (14:00-17:00 LT) were lost due to an
115 instrument malfunction. To fill the data gap, we utilized shortwave solar radiation data from a
116 nearby moored surface buoy, operated by the Ocean Climate Stations (OCS) group at Pacific
117 Marine Environmental Laboratory of the National Oceanic and Atmospheric Administration
118 (PMEL-NOAA). All mooring data are available from the NOAA OCS website
119 (<http://www.pmel.noaa.gov/OCS>). We aligned the two sets of irradiance data (ship-based and
120 surface mooring) and extrapolated over the 3 hour gap in order to obtain consistent E_0^+ for the
121 timespan of the diurnal experiment. Surface reflectance was calculated as a function of solar
122 zenith angle following Kirk (2011) using the R package 'phytotools' (Silsbe, 2015). Subtracting
123 surface reflectance provides PAR just under the air-ocean interface (E_0^-). PAR at 5 m depth
124 (E_{5m}^-) was calculated as $E_{5m}^- = E_0^- \exp^{(k_d \times 5m)}$.

125 Macro-nutrients (P, N, Si) were measured on samples from 2 CTD-rosette casts following the
126 methods outlined in Barwell-Clarke (1996). Additional measurements of surface water (~ 5 m)
127 temperature and salinity were derived from the ship's thermosalinograph (TSG) connected to a
128 continuous seawater supply, and also from the NOAA mooring.

129 **2.2 Sample collection**

130 Seawater samples were collected from the seawater intake system (ca 5 m depth) every 3 hours
131 over a 24 hour period and processed immediately for a variety of physiological assays described
132 below. The resulting dataset consists of 8 time-points (TPs). Local sunrise, solar noon and sunset
133 were at 6:30, 14:40 and 22:50, respectively, resulting in 3 night-time TPs (3:00, 23:00, 0:00) and
134 5 day-time TPs (6:00, 9:00, 12:00, 15:00, 18:00). Samples taken at each TP are summarized in
135 Table 1.

136 **2.3 [chl a] and HPLC**

137 At each TP, duplicate 500 ml samples for [chl a] were filtered onto pre-combusted 25 mm glass
138 fiber filters (GF/F) using low vacuum pressure (<5 mm Hg), taking care to keep the filters out of
139 direct light. Filters were stored at -20 °C and analyzed following the method of Welschmeyer
140 (1994) within two weeks of collection. At 4 TPs (3:00, 9:00, 15:00, 21:00) duplicate 2.2 L
141 samples for pigment analysis were filtered onto pre-combusted 25 mm GF/F, as above. Filters

142 were blotted dry with absorbent paper, flash frozen in liquid nitrogen and stored at -80 °C until
143 analysis by reverse-phase high pressure liquid chromatography (HPLC) following the method of
144 (Pinckney, 2013). The identified pigments were grouped into photosynthetic carotenoids (PSC),
145 photoprotective carotenoids (PPC) and total chlorophyll (TChl) as outlined in Table 2. Ratios of
146 these pigment groups were used to assess diurnal changes in the extent of light stress
147 experienced by the whole phytoplankton assemblage. Xanthophyll cycling (XC) pigments of
148 chromophytes (diatoxanthin (Dt) and diadinoxanthin (Dd)) as well as xanthophyll cycling
149 pigments of prasinophytes and chlorophytes (violaxanthin (Viol) and zeaxanthin (Zea)) were
150 assessed with regard to their relative abundance ((Dt+Dd)/chl *a* and (Zea+Viol)/chl *a*), and de-
151 epoxidation state ratios (DES, Dt/(Dt+Dd) and Zea/(Zea+Viol)). Furthermore, pigment data were
152 used to estimate the relative abundance of different phytoplankton taxa at our sampling site.
153 CHEMTAX analysis was performed using the averaged pigment concentrations from each TP.
154 Analysis was performed essentially as described in Taylor et al. (2013). The initial pigment ratio
155 matrix, specific to North Pacific phytoplankton isolates, was taken from Table 5 in Lee et al.
156 (2011).

157 **2.4 Absorption spectra**

158 Absorption spectra of phytoplankton cellular pigments ($a_{phy}(\lambda)$) were determined following
159 the quantitative filter technique (QFT) as described in (Mitchell et al., 2002). At each TP,
160 duplicate 1.1 L samples were filtered onto pre-combusted 25 mm GF/F under low vacuum
161 pressure and light, taking care to achieve even sample distribution on the filter. Reference filters
162 were prepared by filtering 1.1 L of Milli-Q water. Filters were carefully placed into 25 mm tissue
163 capsules (Fisher), flash frozen in liquid nitrogen and stored at -80 °C until analysis within 1
164 month of the experiment. Sample filters were analyzed on a Cary BIO-100 dual-beam
165 spectrophotometer (Varian) against reference filters as described in Mitchell et al. (2002).
166 Optical density (OD) was measured from 370-800 nm (1 nm resolution) before and after
167 extraction of pigment with 90% methanol (Kishino et al., 1985) to determine OD of the whole
168 particulate sample and OD of detritus after pigment extraction, respectively. Each sample and
169 blank was analyzed in triplicate, to minimize error associated with instrument measurements.
170 The wavelength-specific phytoplankton pigment absorption spectrum ($a_{phy}(\lambda)$, m^{-1}) was
171 calculated as:

172
$$a_{phy}(\lambda) = 2.303 \times \left(OD_{sample}(\lambda) - OD_{detrius}(\lambda) \right) \times \frac{A}{V} \times \beta^{-1} \quad (2)$$

173 where 2.303 is the conversion of from base-10 to a natural logarithm, A is the particulate
 174 retention area of the filter (m^2), V is the volume filtered (m^3), and β is the path-length
 175 amplification coefficient (4.5; Röttgers and Gehnke, (2012)). To determine chl *a* specific
 176 absorption spectra ($a^*_{phy}(\lambda)$, $\text{m}^{-1} \text{ mg chl } a^{-1}$), values were normalized to corresponding [chl *a*]
 177 values. Absorption spectra were used for spectral correction of our rate measurements, as
 178 described in detail below.

179 **2.5 FRRF-derived photophysiological parameters and ETR_{RCII}**

180 All FRRF measurements were conducted on a bench top FRRF instrument (Soliense Inc.), as
 181 described in Schuback et al. (2015). At each TP, background fluorescence blanks were prepared
 182 by gently syringe filtering a small amount of sample through a pre-combusted GF/F. We applied
 183 a single turnover (ST) protocol consisting of an excitation sequence (100 flashlets with 1.0 μs
 184 length and 2.5 μs interval, $46200 \mu\text{mol quantum}^{-2} \text{ s}^{-1}$ peak power intensity, resulting in a
 185 excitation sequence of 250 μs , providing \sim 5-10 quanta per RCII), followed by a relaxation
 186 sequence (50 flashlets with 1.0 μs length and 20 μs interval). Excitation power was provided by
 187 an array of eight LEDs at four wavelengths centered on 445 nm, 470 nm, 505 nm, and 530 nm
 188 (equal intensity from each wavelength, applied simultaneously). We measured steady state light
 189 curves (SSLC), where each sample was exposed to 10 actinic ‘background’ irradiances from 0 to
 190 $1000 \mu\text{mol quanta m}^{-2} \text{ s}^{-1}$, provided at the same four wavelengths. All ChlF yields and
 191 parameters described below were derived by an iterative non-linear fitting procedure, applying
 192 the four parameter biophysical model of Kolber et al. (1998) to a mean of 20 consecutive ST
 193 flashlet sequences using custom software (Z. Kolber). This software accounts for the formation
 194 of fluorescence quenching, most likely due to formation of a P680 triplet, which reduces the
 195 maximum fluorescence yield attainable during the ST flash by 3-6%. Throughout the SSLC, ST
 196 flashlet sequences were measured continuously (1 s interval) and the length of each light step
 197 was optimized to allow all derived parameters to reach steady state (ca 3 min). ChlF yields and
 198 parameters corresponding to each light level were obtained from the mean of the last three
 199 acquisitions at each light level. In this way, we derived the fluorescence yields F_o and F_m (in

200 dark-regulated state) as well as F' and F_m' (in the light regulated state for each light level of the
201 SSLC). F_o' was calculated as $F_o' = F_o / (F_v / F_m + F_o / F_m')$ (Oxborough and Baker, 1997).

202 The five fluorescence yields F_o , F_m , F' , F_m' and F_o' were used to calculate ChlF parameters,
203 following Roháček (2002) as described in Schuback et al. (2015). Furthermore, the functional
204 absorption cross section of PSII, σ_{PSII} ($\times 10^{-20} \text{ m}^2 \text{ RCII}^{-1}$), was derived from the rate of closure of
205 RCII in the dark-regulated and each light-regulated state (Kolber and Falkowski, 1993; Kolber et
206 al., 1998). We calculated ETR_{RCII} as:

$$207 \quad ETR_{RCII} = E \times \sigma'_{PSII} \times \frac{F_q'}{F_v'} \times \Phi_{RC} \times 6.022 \times 10^{-3} \quad (3)$$

208 where E ($\mu\text{mol quanta m}^{-2} \text{ s}^{-1}$) is the actinic irradiance at each light level, σ'_{PSII} ($\times 10^{-20} \text{ m}^2 \text{ RCII}^{-1}$)
209 is the functional absorption cross section of PSII at each light level, and F_q'/F_v' is the quantum
210 efficiency of photochemical energy conversion in RCII at a given light intensity. The parameter
211 F_q'/F_v' can also be interpreted as an estimate of the fraction of RCII in the open state, i.e. the
212 primary stable electron acceptor in the oxidized state (Roháček, 2002). The parameter Φ_{RC} (mol
213 $\text{e}^- \text{ mol photon}^{-1}$) has the constant value of 1, given that for each photon absorbed and delivered to
214 RCII, one electron is transferred from P_{680} to Q_A (Kolber and Falkowski, 1993). The number
215 6.022×10^{-3} converts $\mu\text{mol quanta}$ to quanta and 10^{-20} m^2 to m^2 .

216 We additionally calculated ETR_{RCII} using the alternative approach

$$217 \quad ETR_{RCII} = E \times \sigma_{PSII} \times \frac{(F_q'/F_m')}{(F_v/F_m)} \times \Phi_{RC} \times 6.022 \times 10^{-3} \quad (4)$$

218 Both calculations are equivalent, assuming that non-photochemical quenching processes
219 affecting ChlF can be adequately accounted for in either the absorption term (Eq. 3) and the
220 efficiency term (Eq. 4). The difference between ETR_{RCII} values calculated in both ways ($n=71$)
221 was negligible, ranging from 1 % to 16 % with a mean coefficient of variance of 6 %.

222 The parameter τ (ms) is the time constant of re-oxidation of the primary stable electron
223 acceptor Q_A and was estimated from the relaxation sequence of the ST protocol. We used values
224 of τ , estimated for the dark-regulated state at each TP, to derive estimates of the rate of Q_A re-
225 oxidation ($1/\tau$; ms^{-1}). Non-photochemical quenching (NPQ) at each light level was estimated as
226 the so-called normalized Stern-Volmer quenching coefficient, $NPQ_{NSV} = (F_m'/F_v') - 1 = F_o'/F_v'$
227 (McKew et al., 2013). This alternative approach to the more common estimate of NPQ ($(F_m -$

228 $F_m')/F_m'$; Bilger and Björkman, 1990) represents the ratio of total non-photochemical energy
229 dissipation in the light-regulated state to the rate constant of photochemistry (McKew et al.,
230 2013).

231 **2.6 Carbon fixation**

232 Rates of carbon fixation were measured as small volume PvsE curves in a custom built
233 photosynthetron as described in Schuback et al. (2015). Briefly, 300 mL water samples were
234 spiked with 5.55 MBq NaH¹⁴CO₃ (final concentration 18.5 kBq mL⁻¹, 1.9425 GBq mL⁻¹ specific
235 activity) (Perkin-Elmer). All sample manipulations were conducted under low light. Samples
236 were spiked with tracer within 30 minutes of sampling, mixed gently but thoroughly, and then
237 aliquoted into 20 ml glass scintillation vials and placed into the photosynthetron. The total ¹⁴C
238 activity added was determined from three 1 mL aliquots of the spiked sample added to 1 mL of 1
239 M NaOH. Additionally, 3 time-zero samples were taken for each curve by filtering 20 mL
240 immediately after adding the spike. During the incubations, temperature was kept within 1 °C of
241 in situ temperature by circulating water from a water-bath through an aluminum cooling jacket.
242 Each PvsE curve consisted of 11 light levels spanning intensities from 3 to 600 μmol quanta m⁻²
243 s⁻¹. Incubations lasted for 3.5 hours and were ended by gentle filtration onto pre-combusted 25
244 mm GF/F filters. Given the length of the incubations and the likely slow growth rate of the iron-
245 limited phytoplankton assemblage sampled, our approach likely reflects a rate closer to net rather
246 than gross primary productivity (e.g. Halsey et al., 2011; Pei and Laws, 2013).

247 Filters were stored in scintillation vials at -20 °C until processing within 1 month of the
248 experiment. During laboratory processing, 500 μL of 3 M HCl was added to each filter and vials
249 were left to degas for >24 hours to eliminate any inorganic ¹⁴C remaining in the samples. Ten
250 mL of scintillation cocktail (Scintisafe plus, Fisher) were added to each vial, and vials were then
251 vortexed and left to stand in the dark for >12 hours before analysis on a liquid scintillation
252 counter (Beckman). Disintegrations per minute (DPM) were derived from scintillation counts
253 using a quench curve prepared from commercial ¹⁴C standards (Perkin-Elmer). DPM were
254 converted to units of carbon biomass following Knap et al. (Knap et al., 1996).

255 **2.7 Spectral correction and curve-fitting**

256 To account for differences in the spectral distribution of LEDs used in photosynthetron and
257 FRRF instrument, all rates were divided by a spectral correction factor (SCF).

258
$$SCF = \frac{\sum_{400}^{700} a_{phy}^*(\lambda) E_{in situ}(\lambda) \sum_{400}^{700} E_{LED}(\lambda)}{\sum_{400}^{700} a_{phy}^*(\lambda) E_{LED}(\lambda) \sum_{400}^{700} E_{in situ}(\lambda)} \quad (5)$$

259 where $a_{phy}^*(\lambda)$ (m^{-1}) is the [chl *a*] specific phytoplankton pigment absorption spectrum
 260 determined for each TP as described above, E_{LED} is the spectral distribution of the LEDs used in
 261 photosynthetron or FRRF, and E_{insitu} is the spectral distribution of sunlight at 5 m depth. We
 262 estimated the in situ spectral distribution of PAR at 5 m depth following Stomp et al., 2007 as

263
$$E(\lambda, z) = E_0(\lambda) \exp(-[K_w(\lambda) + K_{GT}(\lambda) + K_{PH}(\lambda)]z). \quad (6)$$

264 Here, $E_0(\lambda)$ is the spectral distribution of incident sunlight and $K_w(\lambda)$ (m^{-1}) is the absorption
 265 by pure water (Pope and Fry, 1997). $K_{GT}(\lambda)$ (m^{-1}) is the absorption by dissolved and particulate
 266 organic matter, estimated as $K_w(\lambda) = K_{GT}(440)\exp(-S(\lambda - 440))$, assuming that
 267 $K_{GT}(440)=0.003\text{ m}^{-1}$, a typical value of clear open ocean water (Morel et al., 2007), and $S=0.017$
 268 nm^{-1} (Kirk, 2010). Values for $K_{PH}(\lambda)$ (m^{-1}) were taken from the absorption spectra measured
 269 using the filter pad technique as described above.

270 After spectral correction, carbon fixation and ETR_{RCII} data were plotted against irradiance
 271 and fit to the exponential model of Webb et al. (1974) using a non-linear least squares regression
 272 procedure in MATLAB. For the carbon fixation data, an intercept parameter was added to force
 273 the regression through the origin and provide a good fit in the linear part of the $P_{vs}E$ curve
 274 (Arrigo et al., 2010; Suggett et al., 2001). For both rates of productivity, we derived the light
 275 saturated maximum rate P_{max} (P_{max} - ETR_{RCII} and P_{max} -C), the light utilization efficiency α (α -
 276 ETR_{RCII} and α -C), and the light saturation point $E_k = P_{max}/\alpha$. When photoinhibition was observed
 277 at high irradiances, the data-points were excluded from the fitting procedure.

278 **2.8 Derivation of conversion factor**

279 The conversion factor linking ETR_{RCII} ($mol\text{ e}^{-} mol\text{ RCII}^{-1} s^{-1}$) and carbon fixation ($mol\text{ C} mol\text{ chl}$
 280 $chl\text{ }a^{-1} s^{-1}$), was derived as described in Schuback et al. (2015);

281
$$\frac{ETR_{RCII} (mol\text{ e}^{-} mol\text{ RCII}^{-1} s^{-1})}{C-fixation (mol\text{ C} mol\text{ chl}\text{ }a^{-1} s^{-1})} = K_c \left(\frac{mol\text{ e}^{-}}{mol\text{ C}} \right) \times 1/n_{PSII} \left(\frac{mol\text{ chl}\text{ }a}{mol\text{ RCII}} \right) \quad (6)$$

282 In this approach, the conversion factor between the two rates accounts for changes in chl *a*
 283 functionally associated with each RCII ($1/n_{PSII}$, $mol\text{ chl}\text{ }a mol\text{ RCII}^{-1}$), as well as variability in

284 the number of charge separations in RCII per CO_2 assimilated (K_c , mol e^- mol C^{-1}). Reported
285 values for K_c range from 1.15 – 54.2 mol e^- mol C^{-1} (Lawrenz et al., 2013) and 200 – 950 mol chl
286 a mol RCII^{-1} for 1/nPSII (Suggett et al., 2010). Consequently, values of K_c/nPSII could be expected
287 to range from 230 - 51490 mol e^- mol C^{-1} mol chl a mol RCII^{-1} .

288 Based on the measured light dependence of carbon fixation and ETR_{RCII} for each sample, we
289 were able to derive the light dependency of the conversion factor K_c/nPSII at each TP.
290 Additionally, we used α and P_{max} values from the ETR_{RCII} and ^{14}C PvsE curves to derive the
291 conversion factor under sub-saturating and saturating light conditions, respectively.

292 **2.9 Relative changes in 1/nPSII**

293 Combining two unknown variables (K_c and 1/nPSII) into one conversion factor, as described
294 above, limits our ability to physiologically interpret observed changes in the coupling of carbon
295 fixation and photosynthetic electron transport. An approach to estimate values of 1/nPSII directly
296 from FRRF measurements has been developed by Oxborough et al. (2012). However, this
297 approach relies on the assumption that the ratio of the rate constants of photochemistry (k_p) and
298 fluorescence (k_f) stay within a narrow range. This assumption is invalidated under conditions of
299 iron limitation, where k_p decreases while k_f increases (e.g. Vassiliev et al., 1995), likely due to
300 the expression of light harvesting complexes that are energetically decoupled from RCII
301 (Behrenfeld and Milligan, 2013; Schrader et al., 2011). Consequently, the approach of
302 Oxborough et al. (2012) should be used with caution when comparing samples over a range of
303 iron limiting conditions.

304 In the current diurnal study, it is likely that the degree of iron limitation experienced by the
305 phytoplankton assemblage stayed relatively constant during our sampling period, such that k_p/k_f
306 values would have remained within a narrow range. Using this rational, we applied a simplified
307 version of the Oxborough et al. (2012) approach to our data, allowing us to estimate relative
308 diurnal changes in 1/nPSII, and, by deduction K_c . In the original approach by Oxborough et al.
309 (2012), changes in of F_o/σ_{PSII} , measured in the dark-regulated state, are multiplied by an
310 instrument specific calibration factor (K_R) to derive absolute values of [RCII]. Lacking this
311 instrument specific calibration factor K_R , we were not able to derive absolute values for [RCII]
312 (and in turn 1/nPSII). However, since K_R is presumed to be constant, we used F_o/σ_{PSII} measured in
313 the dark regulated state at each TP to derive an estimate of relative [RCII] values. These relative

314 [RCII] values were then normalized to [chl *a*] to estimate diurnal changes in 1/nPSII, which were,
315 in turn, used to estimate relative diurnal changes in K_c from measurements of K_c/nPSII.

316 **3 Results**

317 **3.1 Physical and chemical characteristics of the water-column during the**
318 **experiment**

319 During the sampling period, the upper water-column at OSP was stratified, with a well-defined
320 mixed layer of 33 ± 2 m. As expected for iron-limited waters, excess macronutrients were
321 present in the mixed layer and concentrations did not vary over the course of our sampling (2
322 casts, 3:30 and 12:30 local time; N = 9.1 ± 0.00 $\mu\text{mol L}^{-1}$, P = 0.98 ± 0.01 $\mu\text{mol L}^{-1}$, and Si =
323 14.5 ± 0.51 $\mu\text{mol L}^{-1}$). Chlorophyll *a* concentrations were homogenously distributed throughout
324 the mixed layer (0.26 ± 0.03 mg m^{-3} ; 8 depths sampled on 1 cast at 12:30 local time), while
325 temperature was nearly invariant (10.4 ± 0.07 °C) during our sampling period. Total daily
326 incident PAR dose over the 24 h period (E_0^+) was 31.94 mol quanta m^{-2} , with a noon maximum
327 of $1,162 \mu\text{mol quantum}^{-2} \text{s}^{-1}$. The water column light extinction coefficient, k_d, was 0.07 m^{-1} ,
328 which is a value typical for the open ocean (Kirk, 2010). The photic zone (defined as the 0.1%
329 light level) extended below the mixed layer depth at all TPs, apart from the nighttime TP (TPs 1,
330 7 and 8).

331 **3.2 Phytoplankton community composition**

332 CHEMTAX analysis of the pigment data suggested that the phytoplankton assemblage at the
333 sampling location was highly diverse, consisting of approximately 3% diatoms, 2%
334 dinoflagellates, 15% prymnesiophytes, 12% chlorophytes, 16% prasinophytes, 14%
335 cryptophytes, 15% pelagophytes and 23% cyanobacteria.

336 **3.3 Diurnal changes in rates of carbon fixation and ETR_{RCII}**

337 Over the course of the diurnal cycle, we observed significant changes in the PvsE curves for
338 carbon fixation and ETR_{RCII} (Fig. 1). However, the two rates, and their light dependency, did not
339 change in parallel (Fig. 1). As a consequence, we observed significant changes in magnitude and
340 light dependency of the derived conversion factor K_c/nPSII. At all TP, K_c/nPSII increased with

341 increasing light (Fig. 1). The maximum, light-saturated value of K_c/n_{PSII} as well as the slope of
342 the light dependent increase was highest in the afternoon, with maximum K_c/n_{PSII} values (>9000
343 mol e⁻ mol C⁻¹ mol chl *a* mol RCII⁻¹) observed (Fig. 1).

344 From the PvsE curves shown in Fig. 1 we derived the photosynthetic parameters P_{max} and α for
345 both ETR_{RCII} and carbon fixation (Fig. 2c-f). Over the diurnal cycle, the P_{max} -ETR_{RCII} changed
346 by a factor of 3.2 and closely followed the incident irradiance (Fig. 2c), with peak values
347 observed around solar noon. In contrast, P_{max} -C was highest in the early morning and then
348 steadily declined over the course of the day, changing by a factor of 2.5 over the diurnal cycle
349 (Fig. 2e). The conversion factor K_c/n_{PSII} , derived for light saturated photosynthesis (P_{max} -
350 ETR_{RCII}/ P_{max} -C), exhibited high values and a pronounced diurnal cycle, varying by a factor of 2.9
351 (Fig. 2g). Minimum values of K_c/n_{PSII} were observed early in the morning, while maximum
352 values were observed during the afternoon.

353 The light use efficiency per incident quanta under sub-saturating light conditions, α , showed
354 similar patterns to P_{max} for both ETR_{RCII} and carbon fixation (Fig. 2). Values for α -ETR_{RCII}
355 peaked during the late morning and then declined during the afternoon and into the evening (Fig.
356 2d). In contrast, α -C was highest before sunrise and steadily decreased throughout the day (Fig.
357 2f). Over the course of the diurnal cycle, α -ETR_{RCII} changed by a factor of 1.9 while α -C
358 changed by a factor of 3.1. As with P_{max} , the conversion factor K_c/n_{PSII} derived for α , varied
359 strongly (2.4 fold) over the diurnal cycle and showed maximum values during the afternoon, in
360 conjunction with the highest incident PAR levels (Fig. 2h). At all TP, the conversion factor
361 K_c/n_{PSII} was higher during light saturated photosynthesis (P_{max}) than under conditions of light
362 limitation (α) (Fig. 2g and 2h, note different scale of y-axis).

363 The light saturation point E_k was higher for ETR_{RCII} than for carbon fixation at all TPs
364 (Fig. 3), implying that carbon fixation rates saturated at lower light intensity than ETR_{RCII}. For
365 both, carbon fixation and ETR_{RCII}, P_{max} and α changed roughly in parallel (Fig. 2 c, d and 2 e, f).
366 Consequently, diurnal changes in E_k , derived as P_{max}/α , were relatively small (Fig. 2i).
367 Furthermore, the relatively low values of E_k (~ 100 - 150 μ mol quantum⁻² s⁻¹) indicate that both,
368 ETR_{RCII} and carbon fixation, were saturated at in situ irradiance levels for most of the day (Fig.
369 2i).

370 Using the PvsE curves measured for both ETR_{RCII} and carbon fixation (Fig. 1), we derived rates
371 corresponding to the in 5 m irradiance levels at each TP (Figs. 3b and 3c). Over the diurnal

372 cycle, these derived in situ rates of ETR_{RCII} changed by a factor of 5.1 (Fig. 3b), closely
373 following changes in ambient irradiance levels (Fig. 3a), with peak values around noon. By
374 comparison, carbon fixation derived for in situ light levels at 5 m depth changed by a factor of
375 1.7 over the period of our sampling (Fig. 3c). The maximum rate of realized carbon fixation at 5
376 m depth ($0.0433 \pm 0.0112 \text{ mol C mol chl } a^{-1} \text{ s}^{-1}$) was reached in the morning, well before the
377 daily irradiance maximum (Figs. 3a and 3c). The derived in situ conversion factor K_c/n_{PSII} varied
378 by a factor of 3.4. Lowest derived values of in situ K_c/n_{PSII} were observed early in the morning
379 after which values increased until reaching a maximum in the afternoon (Fig. 3d).

380 **3.4 Relative changes in $1/n_{PSII}$**

381 Relative values of $1/n_{PSII}$, shown in Fig. 4a, were highest in the early morning, and then
382 declined by 37% through the afternoon, with lowest values observed at midnight (Fig. 4a). The
383 magnitude of diurnal change in $1/n_{PSII}$ was significantly less than the diurnal changes observed
384 in K_c/n_{PSII} , which were 245% at in situ irradiances (Fig. 4b), 185% at light saturation (P_{max} ; Fig.
385 4c) and 138% at light limitation (α , Fig. 4d). We examined K_c -specific variability by
386 normalizing K_c/n_{PSII} estimates to the relative changes in $1/n_{PSII}$. As shown in Fig. 4, the derived
387 relative changes in K_c showed a diel pattern very similar to that observed for K_c/n_{PSII} at in situ
388 irradiances (Fig. 4b), at light saturation (P_{max} , Fig 4c), and under light limitation (α , Fig. 4d).
389 This result indicates that changes in K_c were the primary drivers of observed variability in
390 K_c/n_{PSII} .

391 **3.5 Photo-regulatory changes**

392 In addition to the apparent diurnal changes in carbon fixation and ETR_{RCII} , we observed strong
393 diurnal oscillations in a number of photophysiological parameters, as well as changes in pigment
394 composition of the phytoplankton assemblage. While higher resolution pigment data would have
395 been desirable, the changes in pigment ratios shown in Fig. 5 indicate that the phytoplankton
396 assemblage sampled from 5 m depth experienced supersaturating light conditions for a
397 substantial part of the day.

398 The ratio of photo-protective carotenoids (PPC) to total pigment (TPig), changed by a factor of
399 1.4 over the diurnal cycle, with lowest values observed at the pre-dawn TP (3:00) and highest in
400 the afternoon (15:00) (Fig. 5a). Similarly, the proportion of xanthophyll cycling (XC) pigments
401 to total chl a increased from pre-dawn (3:00) to mid-afternoon (15:00). This increase was

402 observed in XC pigments specific to chromophytes (42% increase in (Dd+Dt)/chl *a*, Fig. 5b) as
403 well as chlorophyte and prasinophyte-specific XC pigments (17% increase in (Zea+Viol)/chl *a*,
404 Fig 5c). Changes in relative abundance of XC pigments indicate that a higher proportion of the
405 pigment pool is dedicated to photoprotection.

406 In addition to changes in XC pigments, we also observed a 2.4-fold increase in the DES ratio
407 (Dt/(Dd+Dt)) of chromophyte algae between 3:00 and 15:00 (Fig. 5b), and a 1.8-fold increase in
408 the DES ratio of chlorophytes and prasinophytes (Zea/(Zea+Viol), Fig. 5c, The changes in the
409 DES ratio are an indicator of the activation of the photoprotective XC process (Brunet et al.,
410 2011). Our results should be considered as conservative estimates of the DES ratios, given the
411 potential for reversal of the high light induced de-epoxidation during sample processing (samples
412 were exposed to low light for approx. 30 – 60 min during sample collection and filtration).
413 Notwithstanding the relatively low temporal resolution of our pigment samples, the observed
414 changes in pigment ratios indicate that the phytoplankton assemblage sampled from 5 m depth
415 experienced super-saturating light conditions for a substantial part of the day.

416 Further evidence for super-saturating light conditions in the mixed layer comes from
417 observations of diurnal changes in PSII-specific photophysiological parameters derived from
418 FRRF measurements (Fig. 6). Values of F_v/F_m , measured in the dark-regulated state, varied from
419 0.12 to 0.32 and showed an inverse relationship to irradiance (Fig. 6a), likely indicating down-
420 regulation or damage of PSII during high irradiance conditions. The parameter $1/\tau$ (ms^{-1}) is an
421 estimate of the rate of electron transfer from the first stable electron acceptor Q_A to the second
422 stable electron acceptor Q_B . Values of $1/\tau$ varied in parallel with available irradiance over the
423 diurnal cycle, changing approximately 3-fold, and indicating faster electron transport
424 downstream of charge separation in RCII during daylight hours (Fig. 6b). Estimates of the
425 expression of non-photochemical quenching, NPQ_{NSV} , at in situ (5 m depth) irradiance levels
426 changed 7.6-fold over the diurnal cycle, with maximum values near the peak of solar irradiance
427 (Fig. 6c). Spectrally corrected values of the functional absorption cross section of PSII, σ'_{PSII} ,
428 also derived for in situ irradiance levels, correlated inversely with irradiance (Fig. 6d). This
429 decrease further confirms the induction of photo-protective mechanisms within the pigment
430 antenna, preventing excess energy from reaching RCII. Photochemical quenching, estimated as
431 F_q'/F_v' , indicates the fraction of RCII in the ‘open state’, with the primary stable electron
432 acceptor Q_A in the oxidized state (Roháček, 2002). Values of F_q'/F_v' , derived for a reference

433 irradiance value of 500 $\mu\text{mol quanta m}^{-2} \text{ s}^{-1}$ at all TP (F_q'/F_v' (500)), show significant change
434 over the diurnal cycle, with mid-day values twice as high as those observed during the night (Fig.
435 6e).

436 **4 Discussion**

437 The experimental approach and results presented in this study confirm the hypothesized diurnal
438 variation in the coupling of ETR_{RCII} and carbon fixation under iron-limited conditions.

439 Building on the work of others (Behrenfeld et al., 2004, 2008; Halsey and Jones, 2015) we
440 interpret our results in the context of environmentally driven shifts in cellular energy allocation,
441 which decouple photosynthesis from net growth on diurnal timescales. We speculate that the
442 observed patterns are caused by photophysiological plasticity on a molecular level, which
443 enables phytoplankton to maximize growth while minimizing photodamage under iron-limited
444 conditions.

445 In the following, we first discuss diurnal variation at the level of carbon fixation and put our
446 observations in context with the rich information available from the literature. We then consider
447 the diurnal changes in ETR_{RCII} and the derived conversion factor K_c/nPSII , and discuss the
448 relevance of our results to the development of FRRF-based phytoplankton primary productivity
449 measurements.

450 **4.1 Diurnal changes in carbon fixation**

451 Diurnal variations in the capacity ($P_{\text{max}}\text{-C}$), efficiency ($\alpha\text{-C}$) and realized rates of carbon
452 fixation are characteristic of phytoplankton assemblages in the natural environment, and in
453 laboratory cultures (Bruyant et al., 2005; Doblin et al., 2011; Doty and Oguri, 1957; Erga and
454 Skjoldal, 1990; Harding et al., 1981, 1982, 1987; John et al., 2012; MacCaull and Platt, 1977;
455 Prézelin, 1992; Stross et al., 1973; Zhao and Quigg, 2015). The general consensus is that carbon
456 fixation is not passively regulated by the availability of light, but by complex metabolic
457 feedbacks and endogenous circadian rhythms.

458 For example, it has been shown that expression of genes involved in carbon fixation peaks
459 before dawn (Ashworth et al., 2013; Granum et al., 2009), ‘priming’ cells to achieve maximum

460 rates early in the day. High carbon fixation capacities ($P_{max}\text{-C}$) before sunrise, as observed in our
461 data (Fig. 2e), further confirm endogenous circadian control of this pathway.

462 In our data, $P_{max}\text{-C}$ and $\alpha\text{-C}$ peaked early in the morning and co-varied over the diurnal cycle
463 (Fig. 2e and 2f). As a result, E_k (which is derived from the ratio of these parameters) remained
464 relatively constant (Fig. 2i). This ‘ E_k -independent’ variability in the photosynthetic parameters
465 $P_{max}\text{-C}$ and $\alpha\text{-C}$ has long been considered somewhat enigmatic, but is now accepted to be driven
466 by shifts in cellular energy allocation (Behrenfeld et al., 2004, 2008; Bruylants et al., 2005; Halsey
467 and Jones, 2015). In phytoplankton, the fraction of photosynthetically-derived reductant
468 (NADPH) and energy equivalent (ATP) allocated to carbon fixation and net growth as well as
469 the ratio of NADPH:ATP produced are finely tuned to match metabolic demand. Metabolic
470 demand, in turn, is a function of evolved endogenous rhythms and external environmental
471 forcing. As discussed below, the decline in $P_{max}\text{-C}$ (Fig. 2e), $\alpha\text{-C}$ (Fig. 2f), and realized rates of
472 carbon fixation (Fig. 3c) after a peak in the early morning, are likely due to such shifts in energy
473 allocation, and to the damaging effects of excess light, which accumulate throughout the light-
474 period.

475 **4.2 Diurnal changes in ETR_{RCII} and the conversion factor K_c/n_{PSII}**

476 In contrast to the diurnal cycles of $P_{max}\text{-C}$ and $\alpha\text{-C}$, changes in $P_{max}\text{-}ETR_{RCII}$ and $\alpha\text{-}ETR_{RCII}$
477 followed availability of light more closely, peaking around noon (Fig. 2 c,d). Similarly, realized
478 ETR_{RCII} , derived for in situ irradiances at each TP, correlated more closely to light availability
479 than realized rates of carbon fixation (Fig. 3b). While it has been demonstrated that virtually all
480 stages of photosynthesis exhibit circadian control (Suzuki and Johnson, 2001), our results
481 suggests that ETR_{RCII} responds more directly to changes in light availability than the subsequent
482 conversion of light energy into cellular organic carbon. It is important to note that the
483 accumulation of photo-damage and inhibition over the course of the light-period is likely to
484 impart some level of hysteresis to diurnal changes in ETR_{RCII} . Relative to carbon fixation,
485 however, our results show that ETR_{RCII} is much more closely tied to instantaneous changes in
486 light availability. The resulting decoupling of carbon fixation and photosynthetic electron
487 transport is reflected in the diurnal variability in K_c/n_{PSII} (Figs. 2g, 2h, 3d). Based on our
488 estimates of relative changes in $1/n_{PSII}$ over the diel cycle (Fig. 4), we conclude that the majority
489 of diurnal variability in K_c/n_{PSII} results from changes in K_c .

490 In our dataset, in situ values for K_c/n_{PSII} ranged from 2700 to 9200 mol e⁻ mol C⁻¹ mol chl *a* mol
491 RCII⁻¹. Assuming a constant 1/n_{PSII} of 500 mol chl *a* mol RCII⁻¹ (Kolber and Falkowski, 1993),
492 the derived K_c ranges from 5-18 mol e⁻ mol C, which is within the range of previously reported
493 values (Lawrenz et al., 2013) and above the theoretical minimum of 4 mol e⁻ mol C.

494 The large diurnal variability in ETR_{RCII} and carbon fixation and the highly variable K_c/n_{PSII} ,
495 reflect the integrated growth environment experienced by the sampled phytoplankton
496 assemblage. The lowest values of K_c/n_{PSII} were observed early in the morning (Fig. 3d),
497 indicating that much of the energy harvested from sunlight and converted into chemical energy
498 was used directly for carbon fixation. Thereafter, the conversion factor K_c/n_{PSII} increased rapidly,
499 reaching a maximum in the afternoon (Fig. 3d).

500 Diurnal variation in K_c/n_{PSII} can result from a number of interconnected cell physiological
501 mechanisms aimed at re-balancing of energy and/or reductant. Firstly, it is possible that diurnal
502 oscillations in cell metabolism result in changes inorganic carbon respiration and/or excretion. In
503 our 3.5 hours ¹⁴C-uptake experiments, transient organic carbon pools destined for respiration or
504 excretion could have been captured to different extents, affecting the derived conversion factor
505 K_c/n_{PSII} . Changes in cellular energy allocation, controlled in part by endogenous circadian
506 rhythms, could also have affected the conversion factor K_c/n_{PSII} , by re-routing NADPH and ATP
507 generated by the photosynthetic light reaction to processes other than carbon fixation, thus
508 increasing K_c/n_{PSII} . Processes decoupling ETR_{RCII} from carbon fixation include nutrient
509 assimilation (Laws, 1991), carbon concentrating mechanisms (Giordano et al., 2005),
510 photorespiration (Foyer et al., 2009), and malate formation (Halsey and Jones, 2015). Pseudo-
511 cyclic electron transport through the Mehler-ascorbate peroxidase pathway also has the ability to
512 increase the conversion factor K_c/n_{PSII} by allowing ETR_{RCII} to increase without affecting carbon
513 fixation (Miyake and Asada, 2003; Niyogi, 2000). Moreover, processes acting before PSI can
514 decouple ETR_{RCII} and carbon fixation by ‘syphoning’ electrons out of the ETC to alleviate over-
515 reduction under supersaturating light condition. Pseudo-cyclic electron transport though
516 midstream terminal oxidases (Bailey et al., 2008; Mackey et al., 2008), cyclic electron transport
517 around PSII (Feikema et al., 2006; Prasil et al., 1996), and charge recombination in RCII (Vass,
518 2011) could all be important under high mid-day irradiances, increasing ETR_{RCII} without
519 affecting CO₂-assimilation, and thus leading to a higher conversion factor K_c/n_{PSII} .

520 Iron limitation, as experienced by the phytoplankton assemblage we sampled, directly affects
521 the functioning of the ETC, which is rich in iron containing redox-chain components (Raven et
522 al., 1999; Yruela, 2013). It is thus likely that the need for safe dissipation of excess excitation
523 pressure after charge separation in RCII is enhanced under iron limitation (Behrenfeld and
524 Milligan, 2013; Schuback et al., 2015), leading to a greater decoupling of ETR_{RCII} and carbon
525 fixation (Schuback et al., 2015). Pseudo-cyclic electron flow could alleviate over-reduction of
526 the ETC under iron limiting conditions, while also contributing to ATP production (Behrenfeld
527 and Milligan, 2013). The resulting increase in the cellular ATP:NADPH ratio would match the
528 shift in energy demand from growth (higher NADPH requirement) to maintenance (higher ATP
529 requirement), which takes place under nutrient limited growth conditions.

530 While the exact nature and extent of operation of these various pathways and their actual
531 influence on the coupling of ETR_{RCII} and carbon fixation remains to be verified, we suggest that
532 the observed changes in the conversion factor K_c/n_{PSII} over the diurnal cycle reflect the
533 interactions of external phasing of photosynthetic metabolism by the availability of light and
534 internal metabolic rhythms in cell metabolism, which optimize energy allocation and growth
535 under iron-limited conditions.

536 **4.3 Diurnal changes in photophysiology at the level of PSII**

537 In our data, several lines of evidence demonstrate that the phytoplankton assemblage we
538 sampled from 5 m depth experienced supersaturating irradiance during part of the day. A suite of
539 mechanisms was activated to dissipate the excess excitation energy in the pigment antenna,
540 before it could reach RCII. This was indicated by changes in pigment ratios (Fig. 5) and FRRF-
541 derived photophysiological parameters (Fig. 6). The light harvesting antennae of phytoplankton
542 are comprised of both photosynthetic and photoprotective pigments, the relative abundance of
543 which can change in response to irradiance. The ratio $[PPC]/[TPig]$, provides information on the
544 degree of high light acclimation of a mixed phytoplankton assemblage (Brunet et al., 2011). In
545 our data, $[PPC]/[TPig]$ increased during the day (Fig. 5a), indicating that the phytoplankton
546 assemblage experienced and responded to supersaturating irradiance levels. Furthermore,
547 significant changes in the DES ratio of chromophytes ($Dt/(Dt+Dd)$, Fig. 5b), as well as
548 chlorophytes and prasinophytes ($Zea/(Zea+Viol)$, Fig. 5c) illustrate rapid activation of

549 photoprotective energy dissipation in the pigment antenna in response to diurnal changes in
550 irradiance (Brunet et al., 2011).

551 Figure 6 shows pronounced diurnal variability in a number of FRRF derived parameters. Both
552 F_v/F_m (Fig. 6a) and $1/\tau$ (Fig. 6d) were derived for the dark-regulated state at each TP. To reach
553 this dark-regulated state, samples were kept under very low light for a minimum of 30 minutes
554 prior to the measurement. In theory, such low-light incubation allows for oxidation of the ETC
555 and relaxation of all NPQ processes, enabling the measurement of maximum ChlF yields. In
556 practice, however, a fully dark-regulated state cannot be achieved in natural phytoplankton
557 assemblages, where optimal dark-acclimation times can be on the order of hours long (From et
558 al., 2014), and would depend on recent light history and taxonomic composition. Consequently,
559 the interpretation of ChlF yields and parameters in field phytoplankton assemblages should be
560 treated with caution. Notwithstanding these caveats, the FRRF-derived ChlF yields and
561 parameters shown in Fig. 6 show clearly that, at the level of PSII, the sampled phytoplankton
562 assemblage experienced and reacted to excess irradiance.

563 While it is known that nutritional state and taxonomy both strongly influence values of F_v/F_m
564 (Suggett et al., 2009), it is very unlikely that changes in either are responsible for pronounced
565 diurnal cycle of F_v/F_m observed in our data (Fig. 6a). We therefore attribute the mid-day decrease
566 in F_v/F_m to persistent photo-protective changes and photoinhibition in PSII (Öquist et al., 1992).

567 Processes including the light-induced changes in pigment composition shown in Fig. 5, act to
568 dissipate excess excitation pressure in the pigment antenna, before reaching RCII. These
569 processes also quench ChlF yields, as measured by FRRF. Consequently, so-called non-
570 photochemical quenching (NPQ), as estimated from FRRF measurements, has been widely used
571 as an estimate for photoprotective energy dissipation (Demmig-Adams et al., 2014; Derks et al.,
572 2015). NPQ encompasses a wide variety of mechanisms, all acting to dissipate absorbed light
573 energy as heat before it reaches RCII (e.g. Derks et al., 2015). Following the approach of
574 McKew et al. (2013) we estimated NPQ from FRRF measurements as so-called normalized
575 Stern-Volmer quenching (NPQ_{NSV}). The 7.6-fold change in NPQ_{NSV} , estimated for in situ light
576 availability at 5 m depth (Fig. 6b), confirms that the phytoplankton assemblage sampled
577 experienced, and rapidly reacted to, super-saturating light conditions. The inverse light
578 dependence of the functional absorption cross-section of PSII, σ'_{PSII} , derived for in situ

579 irradiances at each TP (Fig. 6c), provides a further illustration of rapid changes taking place in
580 the pigment antenna to prevent excess excitation energy from reaching RCII.

581 In addition to the protective mechanisms acting in the pigment antenna to prevent charge
582 separation in RCII, photo-protective mechanisms also act after charge separation in RCII
583 (section 4.2). These mechanisms alleviate over-reduction by allowing rapid re-oxidation of the
584 primary stable electron acceptor Q_A . Our data show evidence of the up-regulation of such
585 alternative electron sinks during mid-day. Figure 6d shows a light-dependent increase in $1/\tau$,
586 which provides an estimate of the rate of re-oxidation of the first stable electron acceptor Q_A .
587 Increased $1/\tau$ thus suggests faster electron flow downstream from Q_A , which is consistent with
588 the up-regulation of alternative electron sinks. Further support for this idea comes from diel
589 changes in the estimated fraction of Q_A in the oxidized state (F_q'/F_v'), derived for a reference
590 irradiance of $500 \mu\text{mol quanta m}^{-2} \text{ s}^{-1}$ (Fig. 6e). The mid-day increase in the oxidized fraction of
591 Q_A at a constant saturating irradiance of $500 \mu\text{mol quanta m}^{-2} \text{ s}^{-1}$ strongly suggests the up-
592 regulation of alternative electron sinks, which most likely serve a photoprotective function
593 (Mackey et al., 2008). Up-regulation of these photo-protective mechanisms, influences the
594 coupling between electron transport and carbon fixation, and thus directly affects the conversion
595 factor K_c/n_{PSII} (section 4.2).

596 **4.4 Linking K_c/n_{PSII} and NPQ_{NSV}**

597 Excess excitation energy leads to the induction of processes preventing energy transfer to RCII,
598 and to processes acting to prevent over-reduction of the ETC after charge separation. NPQ_{NSV}
599 provides an estimate of thermal energy dissipation upstream of RCII, which acts to prevent
600 excess electron transport and over-reduction of the ETC. Down-stream changes in electron flow
601 after charge separation at RCII are reflected in changes in K_c/n_{PSII} , through the induction of
602 various mechanism, as discussed in the previous section. Following the approach and
603 interpretation suggested by Schuback et al. (2015), we examined the correlation between the
604 derived conversion factor K_c/n_{PSII} and estimates of NPQ_{NSV} . For this analysis, we used estimates
605 of NPQ_{NSV} for each light level and TP of the FRRF light curves and derived values of K_c/n_{PSII} by
606 extrapolation along the carbon fixation and ETR_{RCII} based $P_{vs}E$ curves. As shown in Fig. 7, we
607 found a strong correlation between these two variables ($R^2 = 0.81$, $p\text{-value} < 0.0001$, $n=64$).

608 As described in detail in Schuback et al. (2015), the observed empirical correlation between
609 K_c/n_{PSII} and NPQ_{NSV} can be rationalized in terms of photophysiological mechanisms, acting to
610 dissipate excess excitation energy both upstream and downstream of charge separation in RCII.
611 The dissipation of excess excitation energy as thermal energy before reaching RCII, estimated as
612 NPQ_{NSV} , prevents excess electron transport and over-reduction of the ETC. After the initial
613 charge separation in RCII, excess electron transport and over-reduction of the ETC can be
614 alleviated by a number of alternative electron pathways; the up-regulation of which will increase
615 K_c/n_{PSII} (e.g. Bailey et al., 2008; Cardol et al., 2011; Laureau et al., 2013; Mackey et al., 2008;
616 McDonald et al., 2011; Niyogi, 2000; Streb et al., 2005; Vass, 2011; Zehr and Kudela, 2009).
617 Thus, both NPQ_{NSV} and K_c/n_{PSII} respond strongly to excess excitation pressure, providing a
618 possible mechanistic interpretation for their correlation. In fact, a positive feedback loop exists
619 between energy dissipation in the antenna and photosynthetic control in the ETC, because
620 alternative electron pathways enhance the trans-membrane ΔpH , which triggers several
621 components of NPQ (Nawrocki et al., 2015). The correlation between NPQ_{NSV} and K_c/n_{PSII} is
622 likely to be especially strong under iron limiting conditions, due to the enhancement of energy
623 dissipation mechanisms when the functioning of the ETC is comprised by the availability of iron.

624 While a correlation between NPQ_{NSV} and K_c/n_{PSII} has important implications for the derivation
625 of carbon-based primary productivity rates from FRRF measurements, the correlation can be
626 confounded by ambiguity and inherent biases in the derivation of all involved parameters. For
627 example, while the correlations between NPQ_{NSV} and K_c/n_{PSII} in the present, as well as our
628 previously published dataset (Schuback et al., 2015), are strong, their regression slopes differ.
629 The observed discrepancy could be explained in several ways. Firstly, data in our previous study
630 was not corrected for spectral differences between the FRRF instrument, the ^{14}C -uptake
631 experiments and in situ light. As a consequence, absolute values of the derived conversion factor
632 were likely over-estimated. Furthermore, data presented in Schuback et al. (2015) included
633 phytoplankton assemblages sampled over a range of iron-limited and iron-replete conditions.
634 The resulting variability in phytoplankton growth rates influence the balance between net and
635 gross carbon fixation captured in 3 hour ^{14}C -uptake experiments(Halsey et al., 2011; Milligan et
636 al., 2015; Pei and Laws, 2013), and affect the derived conversion factor K_c/n_{PSII} .

637 More generally, significant uncertainty remains in the estimation of ETR_{RCII} from ChlF yields,
638 particularly if the theoretical biophysical models are applied to mixed phytoplankton

639 assemblages containing species with contrasting photosynthetic architectures and photo-
640 physiological characteristics. Inherent biases and potential systematic errors in the derivation of
641 ETR_{RCII} will inevitably affect the derived conversion factor K_c/n_{PSII} . Similarly, it remains unclear
642 if the quenching of ChlF yields, used to derive NPQ, correlate linearly with increases in thermal
643 energy dissipation in the pigment antenna (Derks et al., 2015). Ultimately, larger datasets,
644 spanning multiple oceanic regions and phytoplankton assemblages of contrasting taxonomic
645 composition and physiological state are needed to further investigate the correlation between
646 NPQ_{NSV} and K_c/n_{PSII} .

647 **5 Conclusion**

648 The lure of FRRF instruments lies in their potential for autonomous, instantaneous data
649 acquisition at high temporal and spatial resolution. However, uncertainty in the conversion
650 factor needed to convert rates of ETR_{RCII} into ecologically relevant rates of carbon fixation
651 remains a significant challenge. Through a suite of photo-physiological data and ancillary
652 measurements, our results provide some insight into the potential mechanistic causes leading to
653 an uncoupling of ETR_{RCII} and carbon fixation over diurnal cycles in iron-limited phytoplankton
654 assemblages. Beyond providing improved methods to estimate phytoplankton carbon fixation
655 rates, information on magnitude and variability of the conversion factor linking ETR_{RCII} and
656 carbon fixation allows a better mechanistic understanding of how phytoplankton harvest and
657 allocate light energy in response to environmental conditions. Our mechanistic understanding of
658 these processes is crucial for the modeling and prediction of patterns in marine primary
659 productivity in the face of climate-dependent changes in oceanic ecosystems.

660 More generally, it is important to consider that the dynamics of marine productivity over
661 long time-scales are ultimately controlled by interactions among biological and physical
662 processes that have strong diurnal components. Several recent studies suggest a previously
663 under-appreciated importance of closely coupled diurnal oscillations as the underlying
664 mechanisms of ecosystem stability in open ocean food webs (Ottesen et al., 2014; Ribalet et al.,
665 2015). Our results show strong diurnal variability in photophysiology and cell metabolism of
666 mixed phytoplankton assemblages. These physiological processes likely influence the phasing

667 and periodicity of higher trophic level processes, and may ultimately contribute to conveying
668 stability to the system.

669

670 **Acknowledgements**

671 The authors thank Marie Robert and the scientific and coast guard crews on board *CCGS*
672 *John P. Tully* during Line-P 2014-18. We would further like to thank Z. Kolber for assistance
673 with the FRRF instrument and C. Hoppe and D. Semeniuk for their critical reading of earlier
674 versions of the manuscript. We furthermore thank three anonymous reviewers for their insightful
675 comments and suggestions.

1 **References**

2 Arrigo, K. R., Mills, M. M., Kropuenske, L. R., Dijken, G. L. van, Alderkamp, A.-C. and
3 Robinson, D. H.: Photophysiology in two major southern ocean phytoplankton taxa:
4 photosynthesis and growth of *Phaeocystis antarctica* and *Fragilariaopsis cylindrus* under
5 different irradiance levels, *Integr. Comp. Biol.*, 50, 950–966, doi:10.1093/icb/icq021, 2010.

6 Ashworth, J., Coesel, S., Lee, A., Armbrust, E. V., Orellana, M. V. and Baliga, N. S.: Genome-
7 wide diel growth state transitions in the diatom *Thalassiosira pseudonana*, *Proc. Natl. Acad.*
8 *Sci.*, 110, 7518–7523, doi:10.1073/pnas.1300962110, 2013.

9 Babin, M., Morel, A., Claustre, H., Bricaud, A., Kolber, Z. and Falkowski, P. G.: Nitrogen- and
10 irradiance-dependent variations of the maximum quantum yield of carbon fixation in eutrophic,
11 mesotrophic and oligotrophic marine systems, *Deep Sea Res. Part Oceanogr. Res. Pap.*, 43,
12 1241–1272, doi:10.1016/0967-0637(96)00058-1, 1996.

13 Bailey, S., Melis, A., Mackey, K. R. M., Cardol, P., Finazzi, G., van Dijken, G., Berg, G. M.,
14 Arrigo, K., Shrager, J. and Grossman, A.: Alternative photosynthetic electron flow to oxygen in
15 marine *Synechococcus*, *Biochim. Biophys. Acta BBA - Bioenerg.*, 1777, 269–276,
16 doi:10.1016/j.bbabi.2008.01.002, 2008.

17 Barwell-Clarke, F.W.: Institute of Ocean Sciences Nutrient Methods and Analysis, *Can. Tech.*
18 *Rep. Hydrogr. Ocean Sci.* , 182, 43 pp., 1996.

19 Behrenfeld, M. J. and Milligan, A. J.: Photophysiological expressions of iron stress in
20 phytoplankton, *Annu. Rev. Mar. Sci.*, 5, 217-246, doi:10.1146/annurev-marine-121211-172356,
21 2013.

22 Behrenfeld, M. J., Prasil, O., Babin, M. and Bruyant, F.: In search of a physiological basis for
23 covariations in light-limited and light-saturated photosynthesis, *J. Phycol.*, 40, 4–25, 2004.

24 Behrenfeld, M. J., Halsey, K. H. and Milligan, A. J.: Evolved physiological responses of
25 phytoplankton to their integrated growth environment, *Philos. Trans. R. Soc. B Biol. Sci.*, 363,
26 2687–2703, 2008.

27 Bilger, W. and Björkman, O.: Role of the xanthophyll cycle in photoprotection elucidated by
28 measurements of light-induced absorbance changes, fluorescence and photosynthesis in leaves of
29 *Hedera canariensis*, *Photosynth. Res.*, 25, 173–185, doi:10.1007/BF00033159, 1990.

30 Brunet, C., Johnsen, G., Lavaud, J. and Roy, S.: Pigments and photoacclimation processes,
31 *Phytoplankton Pigments Charact. Chemotaxon. Appl. Oceanogr.*, available at:
32 <https://hal.archives-ouvertes.fr/hal-01101814/> (last accessed 14 December 2015), 2011.

33 Bruyant, F., Babin, M., Genty, B., Prasil, O., Behrenfeld, M. J., Claustre, H., Bricaud, A.,
34 Garczarek, L., Holtzendorff, J. and Koblizek, M.: Diel variations in the photosynthetic
35 parameters of *Prochlorococcus* strain PCC 9511: Combined effects of light and cell cycle,
36 *Limnol. Oceanogr.*, 50, 850–863, 2005.

37 Cardol, P., Forti, G. and Finazzi, G.: Regulation of electron transport in microalgae, *Biochim.*
38 *Biophys. Acta BBA-Bioenerg.*, 1807, 912–918, 2011.

39 Cheah, W., McMinn, A., Griffiths, F. B., Westwood, K. J., Wright, S. W., Molina, E., Webb, J.
40 P. and van den Enden, R.: Assessing sub-antarctic zone primary productivity from fast repetition
41 rate fluorometry, *Deep Sea Res. Part II Top. Stud. Oceanogr.*, 58, 2179–2188,
42 doi:10.1016/j.dsr2.2011.05.023, 2011.

43 Corno, G., Letelier, R. M., Abbott, M. R. and Karl, D. M.: Assessing primary production
44 variability in the North Pacific Subtropical Gyre: a comparison of fast repetition rate fluorometry
45 and ^{14}C measurements, *J. Phycol.*, 42, 51–60, 2006.

46 Demmig-Adams, B., Garab, G., Adams III, W. and Govindjee (Eds.): *Non-Photochemical*
47 *Quenching and Energy Dissipation in Plants, Algae and Cyanobacteria*, Springer Netherlands,
48 Dordrecht. Available from: <http://link.springer.com/10.1007/978-94-017-9032-1> (last accessed 9
49 June 2015), 2014.

50 Derks, A., Schaven, K. and Bruce, D.: Diverse mechanisms for photoprotection in
51 photosynthesis. Dynamic regulation of photosystem II excitation in response to rapid
52 environmental change, *Biochim. Biophys. Acta BBA - Bioenerg.*, 1847, 468–485,
53 doi:10.1016/j.bbabi.2015.02.008, 2015.

54 Doblin, M. A., Petrou, K. L., Shelly, K., Westwood, K., van den Enden, R., Wright, S., Griffiths,
55 B. and Ralph, P. J.: Diel variation of chlorophyll-*a* fluorescence, phytoplankton pigments and
56 productivity in the Sub-Antarctic and Polar Front Zones south of Tasmania, Australia, *Deep Sea*
57 *Res. Part II Top. Stud. Oceanogr.*, 58, 2189–2199, doi:10.1016/j.dsr2.2011.05.021, 2011.

58 Doty, M. S. and Oguri, M.: Evidence for a photosynthetic daily periodicity, *Limnol. Oceanogr.*,
59 2, 37–40, doi:10.4319/lo.1957.2.1.0037, 1957.

60 Erga, S. R. and Skjoldal, H. R.: Diel variations in photosynthetic activity of summer
61 phytoplankton in Linda aspollene, western Norway, Available from:
62 <http://brage.bibsys.no/xmlui/handle/11250/108310> (last accessed 14 December 2015), 1990.

63 Feikema, O. W., Marosvölgyi, M. A., Lavaud, J. and van Gorkom, H. J.: Cyclic electron transfer
64 in photosystem II in the marine diatom *Phaeodactylum tricornutum*, *Biochim. Biophys. Acta*
65 *BBA - Bioenerg.*, 1757, 829–834, doi:10.1016/j.bbabi.2006.06.003, 2006.

66 Field, C. B., Behrenfeld, M. J., Randerson, J. T. and Falkowski, P.: Primary production of the
67 biosphere: integrating terrestrial and oceanic components, *Science*, 281, 237–240, 1998.

68 Foyer, C. H., Bloom, A. J., Queval, G. and Noctor, G.: Photorespiratory metabolism: genes,
69 mutants, energetics, and redox signaling, *Annu. Rev. Plant Biol.*, 60, 455–484,
70 doi:10.1146/annurev.arplant.043008.091948, 2009.

71 From, N., Richardson, K., Mousing, E. A. and Jensen, P. E.: Removing the light history signal
72 from normalized variable fluorescence (F_v/F_m) measurements on marine phytoplankton, *Limnol.*
73 *Oceanogr. Methods*, 12, 776–783, doi:10.4319/lom.2014.12.776, 2014.

74 Fujiki, T., Suzue, T., Kimoto, H. and Saino, T.: Photosynthetic electron transport in *Dunaliella*
75 *tertiolecta* (Chlorophyceae) measured by fast repetition rate fluorometry: relation to carbon
76 assimilation, *J. Plankton Res.*, 29, 199–208, 2007.

77 Giordano, M., Beardall, J. and Raven, J. A.: CO₂ Concentrating mechanisms in algae:
78 mechanisms, environmental modulation, and evolution, *Annu. Rev. Plant Biol.*, 56, 99–131,
79 doi:10.1146/annurev.arplant.56.032604.144052, 2005.

80 Goto, N., Miyazaki, H., Nakamura, N., Terai, H., Ishida, N. and Mitamura, O.: Relationships
81 between electron transport rates determined by pulse amplitude modulated (PAM) chlorophyll
82 fluorescence and photosynthetic rates by traditional and common methods in natural freshwater
83 phytoplankton, *Fundam. Appl. Limnol. Arch. Fr Hydrobiol.*, 172, 121–134, doi:10.1127/1863-
84 9135/2008/0172-0121, 2008.

85 Granum, E., Roberts, K., Raven, J. A. and Leegood, R. C.: Primary carbon and nitrogen
86 metabolic gene expression in the diatom *Thalassiosira pseudonana* (bacillariophyceae): diel
87 periodicity and effects of inorganic carbon and nitrogen1, *J. Phycol.*, 45, 1083–1092,
88 doi:10.1111/j.1529-8817.2009.00728.x, 2009.

89 Halsey, K. H. and Jones, B. M.: Phytoplankton strategies for photosynthetic energy allocation,
90 *Annu. Rev. Mar. Sci.*, 7, 265–297, doi:10.1146/annurev-marine-010814-015813, 2015.

91 Halsey, K. H., Milligan, A. J. and Behrenfeld, M. J.: Linking time-dependent carbon-fixation
92 efficiencies in *Dunaliella tertiolecta* (chlorophyceae) to underlying metabolic pathways, *J.*
93 *Phycol.*, 47, 66–76, doi:10.1111/j.1529-8817.2010.00945.x, 2011.

94 Harding, L. W., Meeson, B. W., Prézelin, B. B. and Sweeney, B. M.: Diel periodicity of
95 photosynthesis in marine phytoplankton, *Mar. Biol.*, 61, 95–105, doi:10.1007/BF00386649,
96 1981.

97 Harding, L. W., Prezelin, B. B., Sweeney, B. M. and Cox, J. L.: Primary production as
98 influenced by diel periodicity of phytoplankton photosynthesis, *Mar. Biol.*, 67, 179–186, 1982.

99 Harding, L. W., Fisher, T. R. and Tyler, M. A.: Adaptive responses of photosynthesis in
100 phytoplankton: specificity to time-scale of change in light, *Biol. Oceanogr.*, 4, 403–437,
101 doi:10.1080/01965581.1987.10749499, 1987.

102 John, D. E., López-Díaz, J. M., Cabrera, A., Santiago, N. A., Corredor, J. E., Bronk, D. A. and
103 Paul, J. H.: A day in the life in the dynamic marine environment: how nutrients shape diel
104 patterns of phytoplankton photosynthesis and carbon fixation gene expression in the Mississippi
105 and Orinoco River plumes, *Hydrobiologia*, 679, 155–173, 2012.

106 Kaiblinger, C. and Dokulil, M. T.: Application of fast repetition rate fluorometry to
107 phytoplankton photosynthetic parameters in freshwaters, *Photosynth. Res.*, 88, 19–30, 2006.

108 Kirk, J. T. O.: Light and Photosynthesis in Aquatic Ecosystems, Cambridge University Press,
109 Cambridge, UK, 2011.

110 Kishino, M., Takahashi, M., Okami, N. and Ichimura, S.: Estimation of the spectral absorption
111 coefficients of phytoplankton in the sea, Bull. Mar. Sci., 37, 634–642, 1985.

112 Knap, A. H., Michaels, A., Close, A. R., Ducklow, H. and Dickson, A. G.: Protocols for the joint
113 global ocean flux study (JGOFS) core measurements, JGOFS Repr. IOC Man. Guid. No 29
114 UNESCO 1994, 19, available from: <http://epic.awi.de/17559/1/Kna1996a.pdf> (Accessed 15
115 October 2014), 1996.

116 Kolber, Z. and Falkowski, P. G.: Use of active fluorescence to estimate phytoplankton
117 photosynthesis in situ, Limnol. Oceanogr., 38, 1646–1665, doi:10.2307/2838443, 1993.

118 Kolber, Z. S., Prášil, O. and Falkowski, P. G.: Measurements of variable chlorophyll
119 fluorescence using fast repetition rate techniques: defining methodology and experimental
120 protocols, Biochim. Biophys. Acta BBA - Bioenerg., 1367, 88–106, doi:10.1016/S0005-
121 2728(98)00135-2, 1998.

122 Laureau, C., DE Paepe, R., Latouche, G., Moreno-Chacón, M., Finazzi, G., Kuntz, M., Cornic,
123 G. and Streb, P.: Plastid terminal oxidase (PTOX) has the potential to act as a safety valve for
124 excess excitation energy in the alpine plant species *Ranunculus glacialis*, Plant Cell Environ.,
125 doi:10.1111/pce.12059, 2013.

126 Lawrenz, E., Silsbe, G., Capuzzo, E., Ylöstalo, P., Forster, R. M., Simis, S. G. H., Prášil, O.,
127 Kromkamp, J. C., Hickman, A. E., Moore, C. M., Forget, M.-H., Geider, R. J. and Suggett, D. J.:
128 Predicting the electron requirement for carbon fixation in seas and oceans, PLoS ONE, 8,
129 e58137, doi:10.1371/journal.pone.0058137, 2013.

130 Laws, E. A.: Photosynthetic quotients, new production and net community production in the
131 open ocean, Deep Sea Res. Part Oceanogr. Res. Pap., 38, 143–167, 1991.

132 Lee, Y. W., Park, M. O., Kim, Y. S., Kim, S. S. and Kang, C. K.: Application of photosynthetic
133 pigment analysis using a HPLC and CHEMTAX program to studies of phytoplankton
134 community composition, J Korean Soc Ocean., 16, 117–124, 2011.

135 MacCaull, W. A. and Platt, T.: Diel variations in the photosynthetic parameters of coastal marine
136 phytoplankton, Limnol. Oceanogr., 22, 723–731, doi:10.4319/lo.1977.22.4.0723, 1977.

137 Mackey, K. R. M., Paytan, A., Grossman, A. R. and Bailey, S.: A photosynthetic strategy for
138 coping in a high-light, low-nutrient environment, Limnol. Oceanogr., 53, 900–913,
139 doi:10.4319/lo.2008.53.3.0900, 2008.

140 McDonald, A. E., Ivanov, A. G., Bode, R., Maxwell, D. P., Rodermel, S. R. and Hüner, N. P. A.:
141 Flexibility in photosynthetic electron transport: The physiological role of plastoquinol terminal
142 oxidase (PTOX), Biochim. Biophys. Acta BBA - Bioenerg., 1807, 954–967,
143 doi:10.1016/j.bbabio.2010.10.024, 2011.

144 McKew, B. A., Davey, P., Finch, S. J., Hopkins, J., Lefebvre, S. C., Metodiev, M. V.,
145 Oxborough, K., Raines, C. A., Lawson, T. and Geider, R. J.: The trade-off between the light-
146 harvesting and photoprotective functions of fucoxanthin-chlorophyll proteins dominates light

147 acclimation in *Emiliania huxleyi* (clone CCMP 1516), *New Phytol.*, 200, 74–85,
148 doi:10.1111/nph.12373, 2013.

149 Milligan, A. J., Halsey, K. H. and Behrenfeld, M. J.: Advancing interpretations of ^{14}C -uptake
150 measurements in the context of phytoplankton physiology and ecology, *J. Plankton Res.*, 37,
151 692–698, doi:10.1093/plankt/fbv051, 2015.

152 Mitchell, B. G., Kahru, M., Wieland, J. and Stramska, M.: Determination of spectral absorption
153 coefficients of particles, dissolved material and phytoplankton for discrete water samples, *Ocean
154 Opt. Protoc. Satell. Ocean Color Sens. Valid. Revis.*, 3, 231–257, 2002.

155 Miyake, C. and Asada, K.: The Water-Water Cycle in Algae, in *Photosynthesis in Algae*, edited
156 by Larkum A. W. D., Douglas S. E., and Raven J. A., 183–204, Springer, Netherlands, available
157 from: http://link.springer.com/chapter/10.1007/978-94-007-1038-2_9 (Accessed 10 March
158 2015), 2003.

159 Morel, A., Gentili, B., Claustre, H., Babin, M., Bricaud, A., Ras, J. and Tièche, F.: Optical
160 properties of the “clearest” natural waters, *Limnol. Oceanogr.*, 52, 217–229,
161 doi:10.4319/lo.2007.52.1.0217, 2007.

162 Myers, J.: On the algae: thoughts about physiology and measurements of efficiency, in *Primary
163 Productivity in the Sea*, edited by Falkowski, P. G., 1–16, Springer, New York, US, available at:
164 http://link.springer.com/chapter/10.1007/978-1-4684-3890-1_1 (Accessed 28 August 2015),
165 1980.

166 Napoléon, C. and Claquin, P.: Multi-parametric relationships between PAM measurements and
167 carbon incorporation, an in situ approach, *PloS One*, 7, e40284,
168 doi:10.1371/journal.pone.0040284, 2012.

169 Napoléon, C., Raimbault, V. and Claquin, P.: Influence of nutrient stress on the relationships
170 between PAM measurements and carbon incorporation in four phytoplankton species., *PloS One*,
171 8, e66423, doi:10.1371/journal.pone.0066423, 2013.

172 Nawrocki, W. J., Tourasse, N. J., Taly, A., Rappaport, F. and Wollman, F.-A.: The plastid
173 terminal oxidase: its elusive function points to multiple contributions to plastid physiology,
174 *Annu. Rev. Plant Biol.*, 66, 49–74, doi:10.1146/annurev-arplant-043014-114744, 2015.

175 Niyogi, K. K.: Safety valves for photosynthesis, *Curr. Opin. Plant Biol.*, 3, 455–460,
176 doi:10.1016/S1369-5266(00)00113-8, 2000.

177 Öquist, G., Chow, W. S. and Anderson, J. M.: Photoinhibition of photosynthesis represents a
178 mechanism for the long-term regulation of photosystem II, *Planta*, 186, 450–460,
179 doi:10.1007/BF00195327, 1992.

180 Ottesen, E. A., Young, C. R., Gifford, S. M., Eppley, J. M., Marin, R., Schuster, S. C., Scholin,
181 C. A. and DeLong, E. F.: Multispecies diel transcriptional oscillations in open ocean
182 heterotrophic bacterial assemblages, *Science*, 345, 207–212, doi:10.1126/science.1252476, 2014.

183 Oxborough, K. and Baker, N. R.: Resolving chlorophyll a fluorescence images of photosynthetic
184 efficiency into photochemical and non-photochemical components – calculation of qP and
185 F_v'/F_m' without measuring F_o' ; *Photosynth. Res.*, 54, 135–142, doi:10.1023/A:1005936823310,
186 1997.

187 Oxborough, K., Moore, C. M., Suggett, D. J., Lawson, T., Chan, H. G. and Geider, R. J.: Direct
188 estimation of functional PSII reaction center concentration and PSII electron flux on a volume
189 basis: a new approach to the analysis of Fast Repetition Rate fluorometry (FRRF) data, *Limnol*
190 *Ocean. Methods*, 10, 142–154, 2012.

191 Pei, S. and Laws, E. A.: Does the ^{14}C method estimate net photosynthesis? Implications from
192 batch and continuous culture studies of marine phytoplankton, *Deep Sea Res. Part Oceanogr.*
193 *Res. Pap.*, 82, 1–9, doi:10.1016/j.dsr.2013.07.011, 2013.

194 Pinckney, J. L.: HPLC Method - Technical - Estuarine Ecology, available from:
195 <https://sites.google.com/site/jaypinckney/home/protocols-reports> (last accessed 14 December
196 2015), 2013.

197 Pope, R. M. and Fry, E. S.: Absorption spectrum (380–700 nm) of pure water. II. Integrating
198 cavity measurements, *Appl. Opt.*, 36, 8710, doi:10.1364/AO.36.008710, 1997.

199 Prasil, O., Kolber, Z., Berry, J. A. and Falkowski, P. G.: Cyclic electron flow around
200 photosystem II in vivo; *Photosynth. Res.*, 48, 395–410, doi:10.1007/BF00029472, 1996.

201 Prézelin, B. B.: Diel periodicity in phytoplankton productivity, *Hydrobiologia*, 238, 1–35, 1992.

202 Raateoja, M. P.: Fast repetition rate fluorometry (FRRF) measuring phytoplankton productivity:
203 a case study at the entrance to the Gulf of Finland, Baltic Sea, *Boreal Environ. Res.*, 9, 263–276,
204 2004.

205 Raven, J. A., Evans, M. C. W. and Korb, R. E.: The role of trace metals in photosynthetic
206 electron transport in O_2 -evolving organisms, *Photosynth. Res.*, 60, 111–150,
207 doi:10.1023/A:1006282714942, 1999.

208 Ribalet, F., Swalwell, J., Clayton, S., Jiménez, V., Sudek, S., Lin, Y., Johnson, Z. I., Worden, A.
209 Z. and Armbrust, E. V.: Light-driven synchrony of *Prochlorococcus* growth and mortality in the
210 subtropical Pacific gyre, *Proc. Natl. Acad. Sci.*, 201424279, doi:10.1073/pnas.1424279112,
211 2015.

212 Roháček, K.: Chlorophyll fluorescence parameters: the definitions, photosynthetic meaning, and
213 mutual relationships, *Photosynthetica*, 40, 13–29, doi:10.1023/A:1020125719386, 2002.

214 Röttgers, R. and Gehnke, S.: Measurement of light absorption by aquatic particles: improvement
215 of the quantitative filter technique by use of an integrating sphere approach, *Appl. Opt.*, 51,
216 1336–1351, 2012.

217 Schrader, P. S., Milligan, A. J. and Behrenfeld, M. J.: Surplus photosynthetic antennae
218 complexes underlie diagnostics of iron limitation in a cyanobacterium, PLoS ONE, 6, e18753,
219 doi:10.1371/journal.pone.0018753, 2011.

220 Schreiber, U.: Pulse-amplitude-modulation (PAM) fluorometry and saturation pulse method: an
221 overview, Chlorophyll Fluoresc., 19, 279–319, 2004.

222 Schuback, N., Schallenberg, C., Duckham, C., Maldonado, M. T. and Tortell, P. D.: Interacting
223 effects of light and iron availability on the coupling of photosynthetic electron transport and
224 CO₂-assimilation in marine phytoplankton, PLoS ONE, 10, e0133235,
225 doi:10.1371/journal.pone.0133235, 2015.

226 Silsbe, G.: Phytotools: Phytoplankton Production Tools, an R package available on CRAN:
227 <https://cran.r-project.org/web/packages/phytotoools/index.html>, 2015.

228 Streb, P., Josse, E.-M., Gallouët, E., Baptist, F., Kuntz, M. and Cornic, G.: Evidence for
229 alternative electron sinks to photosynthetic carbon assimilation in the high mountain plant
230 species *Ranunculus glacialis*, Plant Cell Environ., 28, 1123–1135, doi:10.1111/j.1365-
231 3040.2005.01350.x, 2005.

232 Stross, R. G., Chisholm, S. W. and Downing, T. A.: Causes of daily rhythms in photosynthetic
233 rates of phytoplankton, Biol. Bull., 145, 200–209, doi:10.2307/1540359, 1973.

234 Suggett, D., Kraay, G., Holligan, P., Davey, M., Aiken, J. and Geider, R.: Assessment of
235 photosynthesis in a spring cyanobacterial bloom by use of a fast repetition rate fluorometer,
236 Limnol. Oceanogr., 46, 802–810, 2001.

237 Suggett, D. J., Maberly, S. C. and Geider, R. J.: Gross photosynthesis and lake community
238 metabolism during the spring phytoplankton bloom, Limnol. Oceanogr., 51, 2064–2076, 2006.

239 Suggett, D. J., Moore, C. M., Hickman, A. E. and Geider, R. J.: Interpretation of fast repetition
240 rate (FRR) fluorescence: signatures of phytoplankton community structure versus physiological
241 state, Mar Ecol Prog Ser, 376, 1–19, 2009.

242 Suggett, D. J., Moore, C. M. and Geider, R. J.: Estimating aquatic productivity from active
243 fluorescence measurements, in: Chlorophyll *a* Fluorescence in Aquatic Sciences: Methods and
244 Applications, edited by: Suggett D. J., Prasil O., and Borowitzka M. A., 103–127, Springer, the
245 Netherlands, 2010.

246 Suzuki, L. and Johnson, C. H.: Algae know the time of day: circadian and photoperiodic
247 programs, J. Phycol., 37, 933–942, doi:10.1046/j.1529-8817.2001.01094.x, 2001.

248 Taylor, R. L., Semeniuk, D. M., Payne, C. D., Zhou, J., Tremblay, J.-É., Cullen, J. T. and
249 Maldonado, M. T.: Colimitation by light, nitrate, and iron in the Beaufort Sea in late summer, J.
250 Geophys. Res. Oceans, 118, 3260–3277, doi:10.1002/jgrc.20244, 2013.

251 Vass, I.: Role of charge recombination processes in photodamage and photoprotection of the
252 photosystem II complex, *Physiol. Plant.*, 142, 6–16, doi:10.1111/j.1399-3054.2011.01454.x,
253 2011.

254 Vassiliev, I. R., Kolber, Z., Wyman, K. D., Mauzerall, D., Shukla, V. K. and Falkowski, P. G.:
255 Effects of iron limitation on photosystem II composition and light utilization in *Dunaliella*
256 *tertiolecta*, *Plant Physiol.*, 109, 963–972, doi:10.1104/pp.109.3.963, 1995.

257 Webb, W. L., Newton, M. and Starr, D.: Carbon Dioxide Exchange of *Alnus rubra*. A
258 Mathematical Model, *Oecologia*, 17, 281–291, 1974.

259 Welschmeyer, N. A.: Fluorometric analysis of chlorophyll *a* in the presence of chlorophyll *b* and
260 pheopigments, *Limnol. Oceanogr.*, 39, 1985–1992, 1994.

261 Williams, P. J. le B., Thomas, D. N. and Reynolds, C. S.: Phytoplankton Productivity: Carbon
262 Assimilation in Marine and Freshwater Ecosystems, John Wiley and Sons., 2008.

263 Yruela, I.: Transition metals in plant photosynthesis, *Met. Integr. Biometal Sci.*, 5, 1090–1109,
264 doi:10.1039/c3mt00086a, 2013.

265 Zehr, J. P. and Kudela, R. M.: Photosynthesis in the Open Ocean, *Science*, 326, 945–946,
266 doi:10.1126/science.1181277, 2009.

267 Zhao, Y. and Quigg, A.: Study of photosynthetic productivity in the Northern Gulf of Mexico:
268 Importance of diel cycles and light penetration, *Cont. Shelf Res.*, 102, 33–46,
269 doi:10.1016/j.csr.2015.04.014, 2015.

270

271

272

273

274

275

276

277

278

279

280

281

282

283

284

285 **Tables and Figures**

286

287 **Table 1: Parameters measures at each time-point during the diurnal experiment.**

Time Point	1	2	3	4	5	6	7	8
Local time	3:00	6:00	9:00	12:00	15:00	18:00	21:00	0:00
[chl _a]	x	x	x	x	x	x	x	x
HPLC	x		x		x		x	
Absorption Spectra	x	x	x	x	x	x	x	x
FRRF measurements	x	x	x	x	x	x	x	x
C-fixation	x	x	x	x	x	x	x	x

288

289

290

291 **Table 2: Phytoplankton pigments used for the derivation of diagnostic pigment ratios.**

292 Pigments identified from HPLC analysis were chlorophyll *c*₃ (Chl *c*₃), chlorophyll *c*₁*c*₂ (Chl
 293 *c*₁*c*₂), 19'butanoyloxyfucoxanthin (19'ButFuc), fucoxanthin (Fuco), 19'hexanoyloxyfucoxanthin
 294 (19'HexFuc), 9'cis-neoxanthin (Neo), prasinoxanthin (Prasino), violaxanthin (Viola),
 295 diadinoxanthin (Dd), alloxanthin (Allox), diatoxanthin (Dt), lutein, zeaxanthin (Zea), chlorophyll
 296 b (Chl *b*), chlorophyll *a* allomer (Chl *a* allomer), chlorophyll *a* + divinyl chlorophyll *a* (Chl *a*),
 297 chlorophyll *a'* (Chl *a* prime), α carotene (α carot), β carotene (β carot).

Pigment group	Pigments
Photoprotective carotenoids (PPC)	Neo + Viola + Dd + Allox + Dt + Lutein + Zea + β carot
Photosynthetic carotenoids (PSC)	19'ButFuc + Fuco + 19'HexFuc + Prasino + α carot
Total chlorophyll (Tchl)	Chl <i>c</i> ₃ + Chl <i>c</i> ₁ <i>c</i> ₂ + Chl <i>b</i> + Chl <i>a</i> allomer + Chl <i>a</i> + Chl <i>a</i> prime
Total pigment (TPig)	PPC + PSC + Tchl

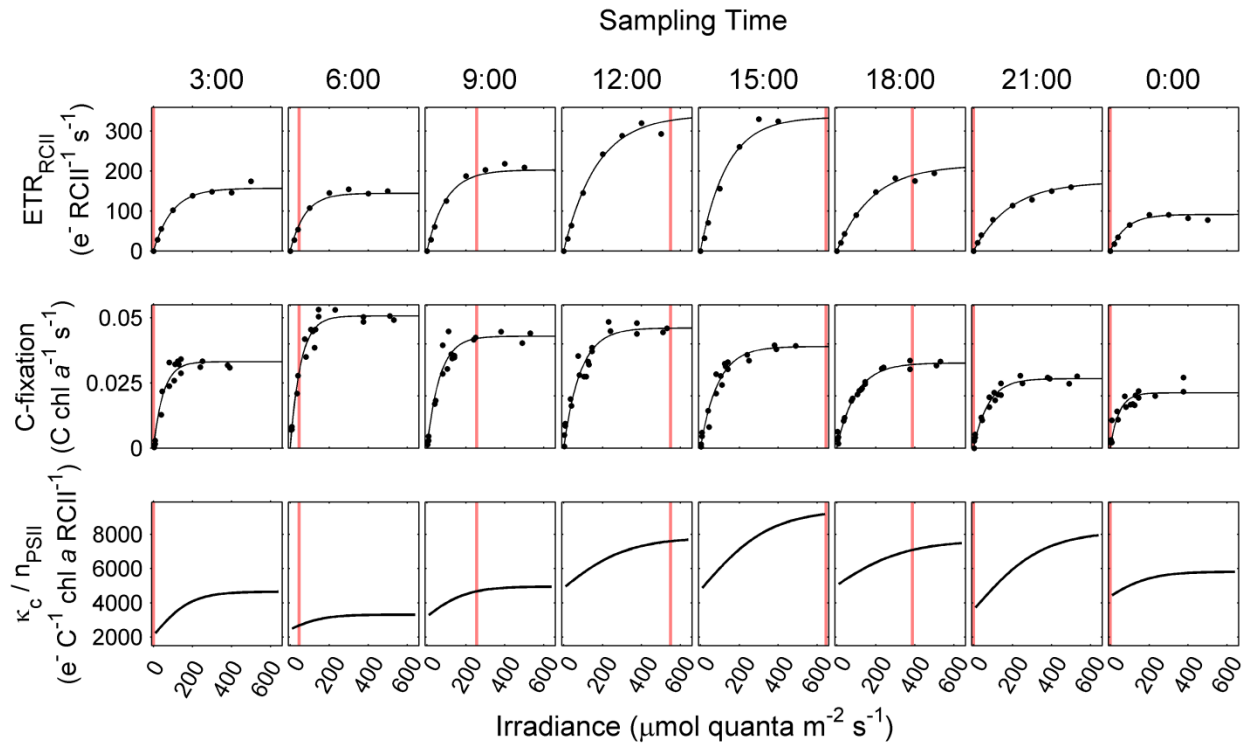
298

299

300

301

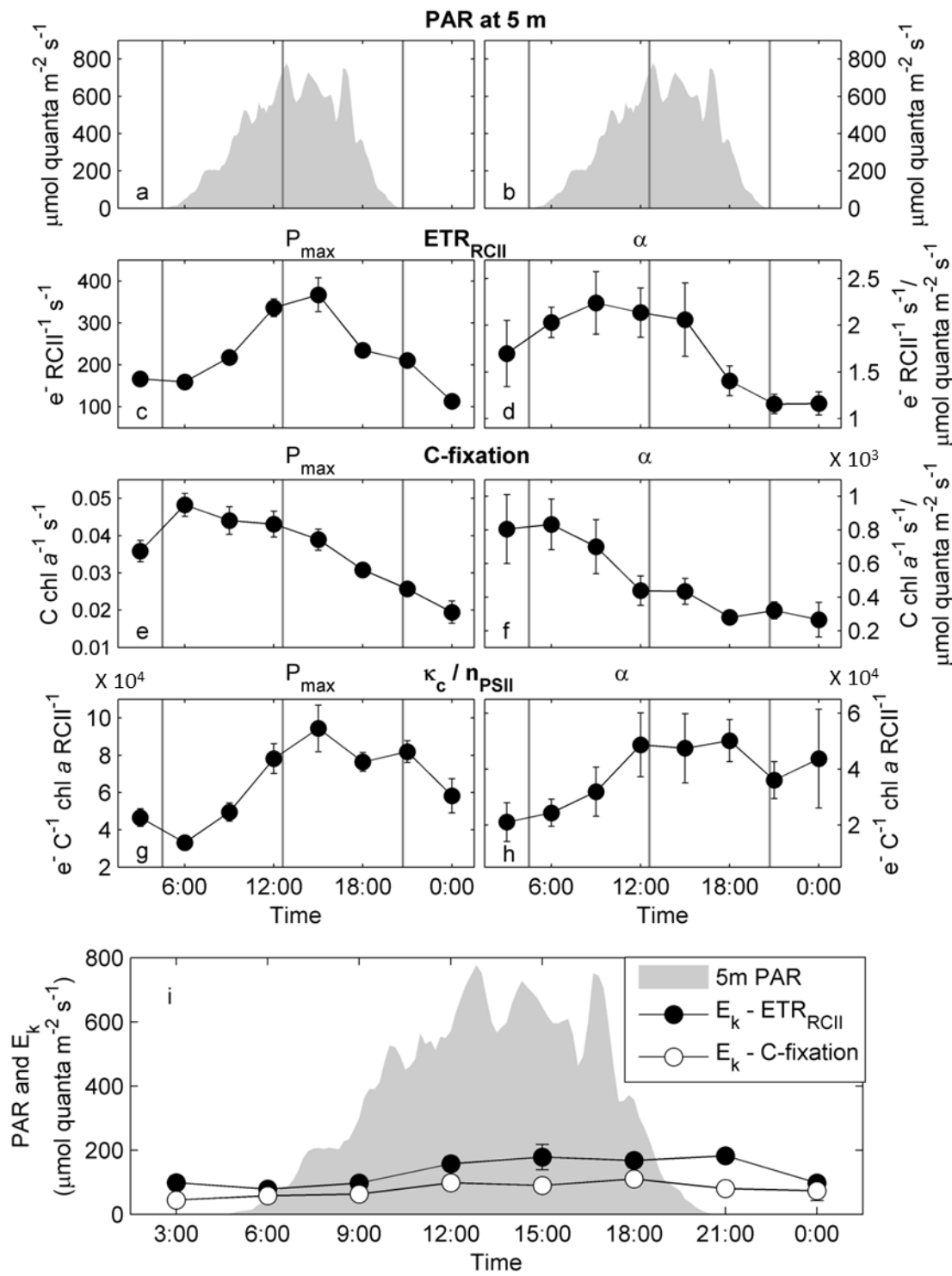
302



303

304 **Figure 1: Diurnal variation in rates and light dependency of ETR_{RCII} , carbon fixation and**
 305 **the derived conversion factor $K_c/nPSII$.** PvsE curves of ETR_{RCII} ($\text{mol e}^- \text{ mol RCII}^{-1} \text{ s}^{-1}$) and
 306 carbon fixation ($\text{mol C mol chl } a^{-1} \text{ s}^{-1}$) were measured at 3 hour intervals over a 24 hour diurnal
 307 cycle. Data were fit to the exponential model of Webb et al. (1974). The conversion factor
 308 $K_c/nPSII$ ($\text{mol e}^- \text{ mol C}^{-1} \text{ mol chl } a \text{ mol RCII}^{-1}$), and its light dependency, were derived as the
 309 quotient of corresponding values of ETR_{RCII} and carbon fixation. The vertical line on plots
 310 corresponds to in situ PAR values at 5 m depth during sampling for each time-point.

311



312

313 **Figure 2: Diurnal changes in capacities and efficiencies of ETR_{RCII} and carbon fixation and**
 314 **the derived conversion factor K_c/n_{PSII}.** The conversion factor K_c/n_{PSII} at light saturation (g) is
 315 derived from the values in (c) and (e). Similarly, the conversion factor K_c/n_{PSII} under light

316 limiting conditions (h) is derived from values in (d) and (f). The error in (b), (c), (e), and (f) is
317 the 95% confidence interval of the parameter derived from the fit to data shown in Fig. 1, and the
318 error in (d) and (g) is the propagated error for (b)/(c) and (e)/(f), respectively. PAR at 5 m depth
319 is shown in (a) and (b). The vertical gray lines in panel (a-h) mark sunrise, solar noon and sunset.
320 Panel (i) shows the light saturation parameter E_k for ETR_{RCII} and carbon fixation in relation to in
321 situ light availability.

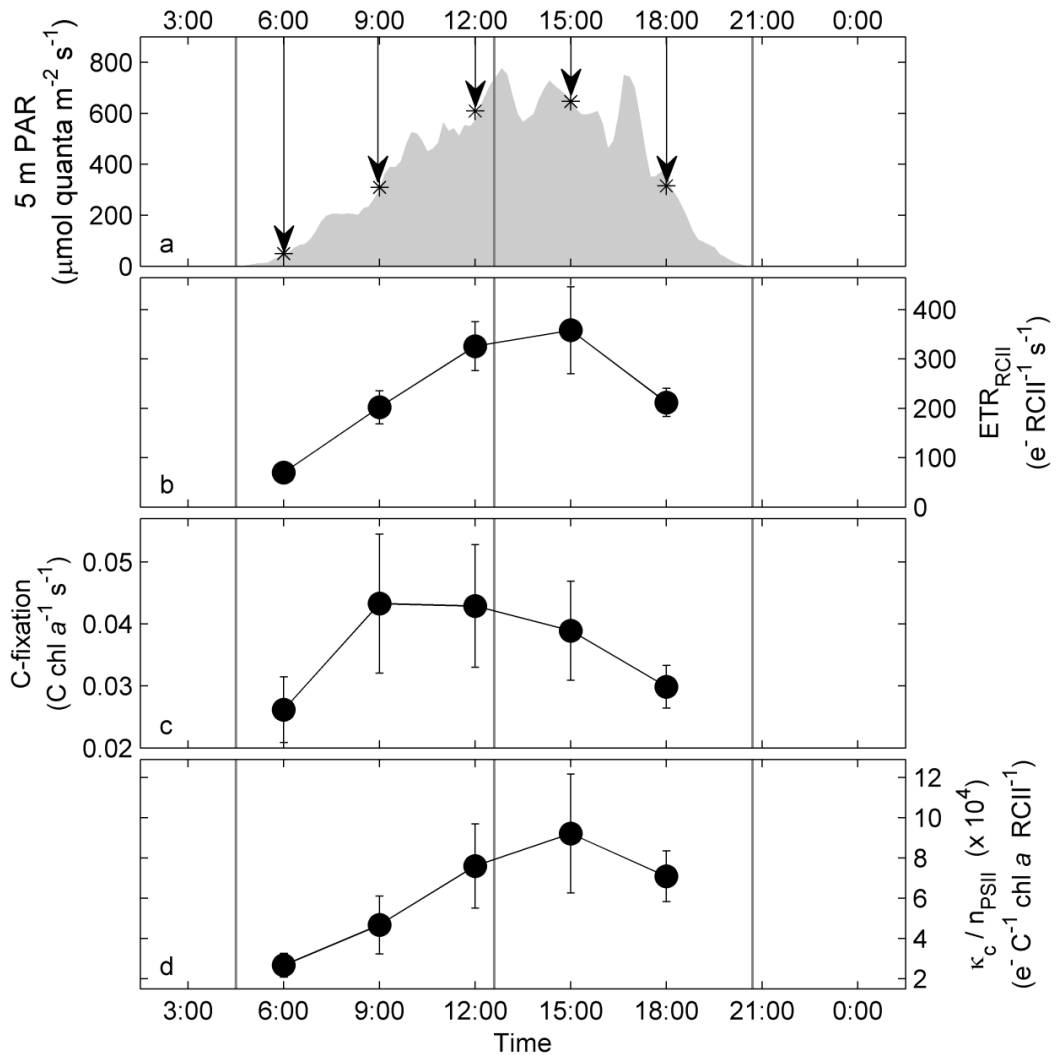
322

323

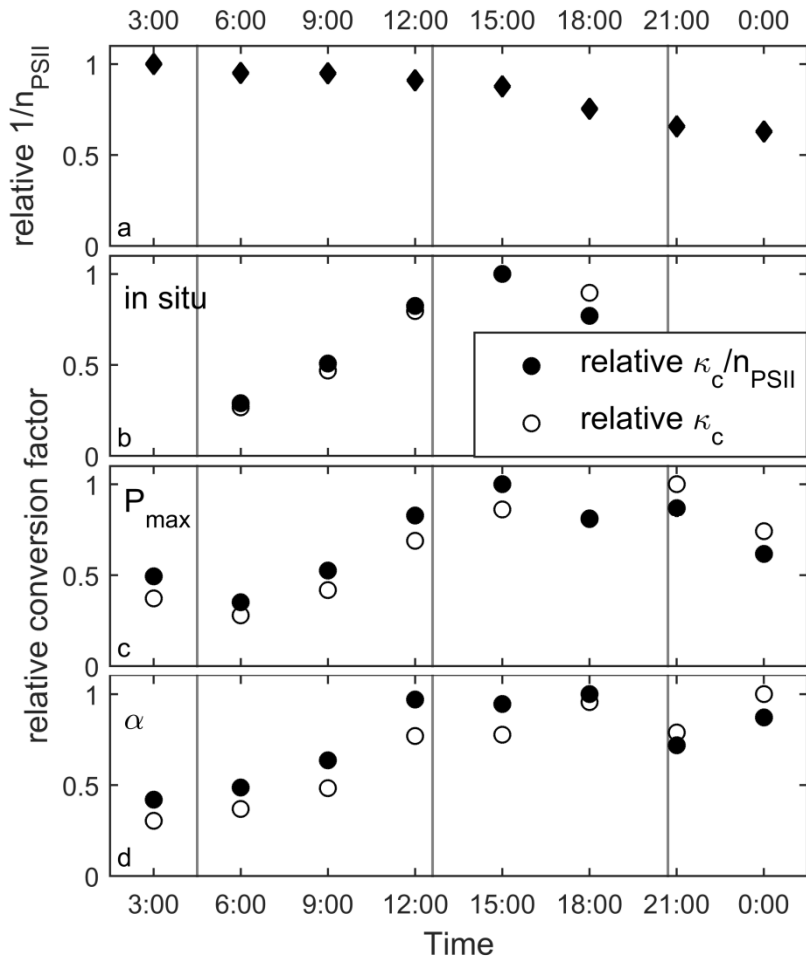
324

325

326

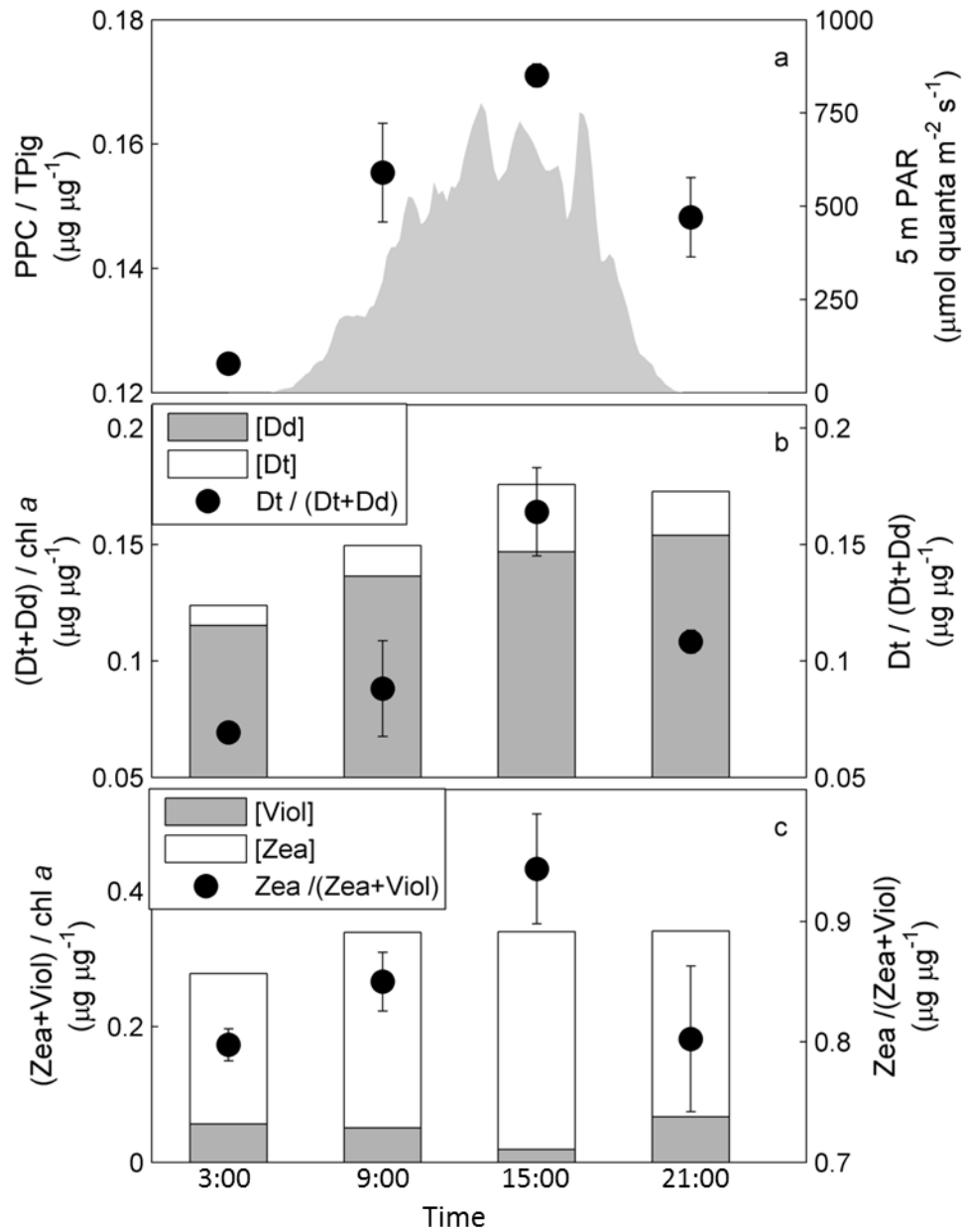


327
328 **Figure 3: Diurnal changes in ETR_{RCII}, carbon fixation and K_c/nPSII derived for in situ light**
329 **intensities at 5 m depth.** Diurnal changes in irradiance at 5 m depth (a), with arrows indicating
330 the PAR value used to derive rates in (b) and (c). Realized rates of ETR_{RCII} (b) and carbon
331 fixation (c) at each time-point were derived from the PvsE relationship established in Fig. 1. The
332 error in (b) and (c) is the propagated 95% confidence interval of the parameter PvsE fit
333 parameters, and the error in (d) is the propagated error from (b)/(c). The vertical gray lines in all
334 plots mark sunrise, solar noon and sunset.



335

336 Figure 4: Relative changes in the components of our conversion factor K_c/n_{PSII} over the diurnal
 337 cycle. Panel (a) shows diurnal changes in $1/n_{PSII}$ (mol chl *a* mol RCII⁻¹), estimated as
 338 $(F_0/\sigma_{PSII})/[chl\ a]$. These relative values of $1/n_{PSII}$ were then used to derive relative values of K_c
 339 (mol e⁻ mol C⁻¹) from values of K_c/n_{PSII} . This was done for the conversion factor derived for in
 340 situ irradiances at 5 m depth (b), the conversion factor derived for light saturated rates (c) and the
 341 conversion factor for light limited rates (d). All values are scaled to 1 for clarity.

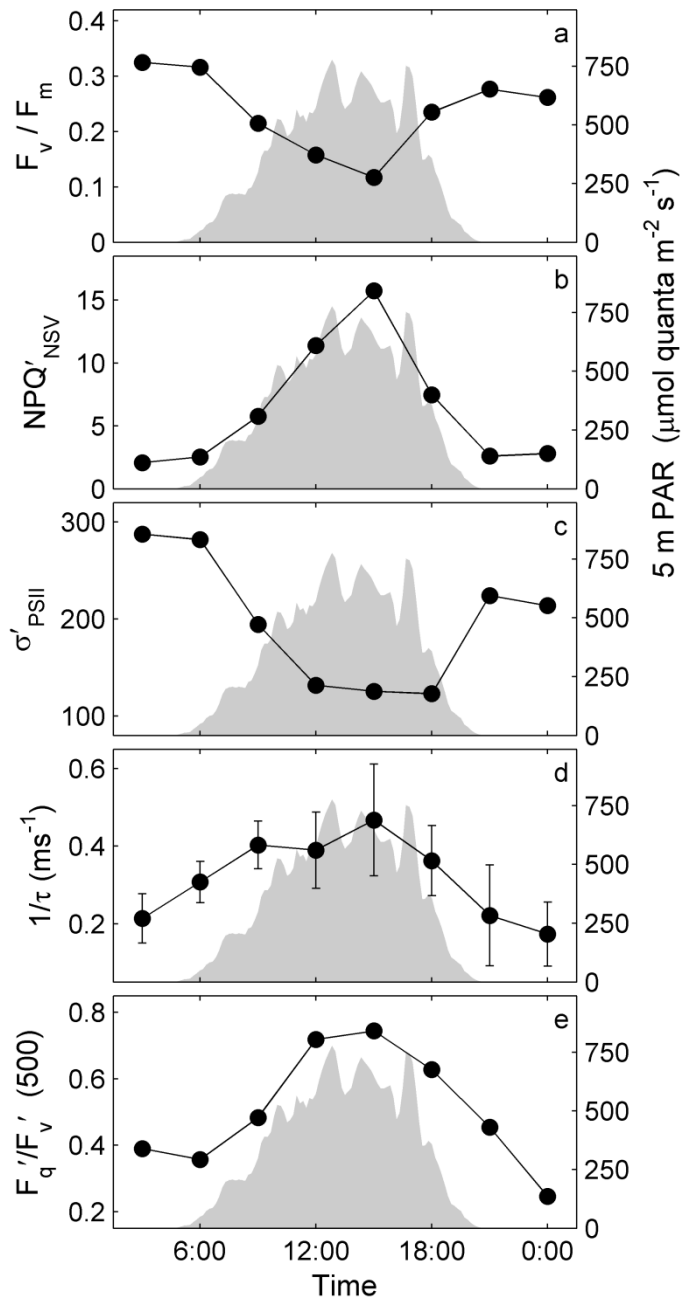


342

343 **Figure 5: Diurnal changes in pigment ratios.** Panel (a) shows changes in the abundance of all
 344 photoprotective pigment (PPC), relative to the total pigment present (TPig) at each time-point.
 345 See Table 2 for a definition of pigment groups used to derive these ratios. Panel (b) shows
 346 relative changes in the abundance of the chromophyte xanthophyll cycling pigments Dd and Dt,
 347 normalized to [chl a]. Changes in the de-epoxidation state ration (DES ratio = $Dt/(Dt+Dd)$), also
 348 shown in (b), indicate the extent of active photo-protective energy dissipation through
 349 xanthophyll cycling in the pigment antenna. Similarly, panel (c) shows xanthophyll cycling

350 pigments Viol and Zea, specific to prasinophytes and chlorophytes. Error bars are the range of
351 values from two replicate samples taken at each time-point.

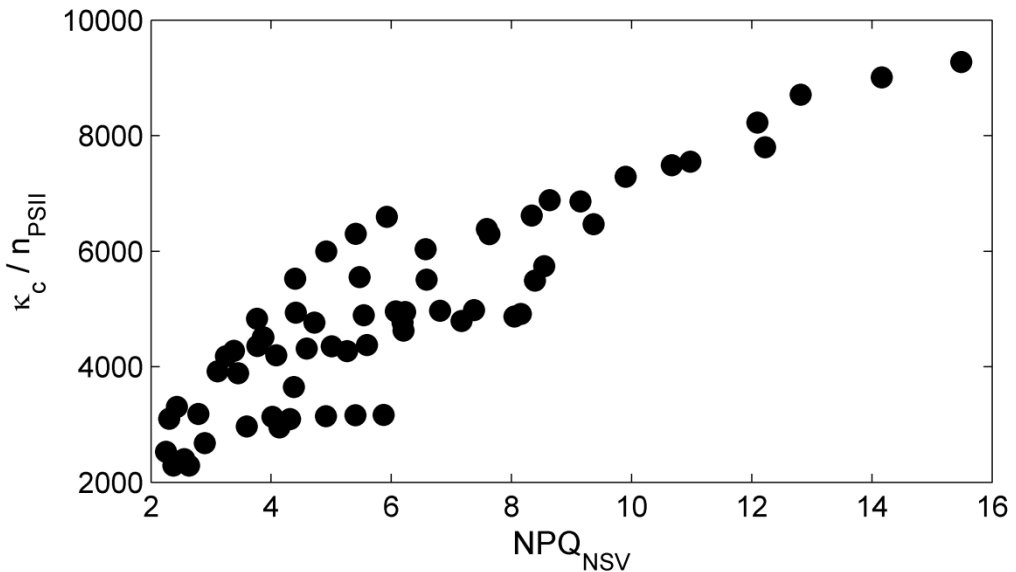
352



353
354 **Figure 6: Diurnal changes in PSII photophysiological parameters derived from FRRF**
355 **measurements.** Panel (a) F_v/F_m in the dark-regulated state at each TP. Panel (b) and (c) show the

356 normalized Stern-Volmer quenching, NPQ_{NSV} , derived as F_o'/F_v' (McKew et al., 2013) and the
 357 functional absorption cross section, σ'_{PSII} , both estimated for in situ light availability at each TP.
 358 Values in (b) and (c) were calculated by extrapolating between values derived for each light step
 359 of the FRRF steady state light curves. Panel (d) shows estimates of the rate of re-oxidation of
 360 Q_A . Panel (c) shows estimates of photochemical quenching (F_q'/F_v'), indicating the fraction of
 361 open RCII (primary stable electron acceptor Q_A oxidized) at a reference irradiance level of 500
 362 $\mu\text{mol quanta m}^{-2}\text{s}^{-1}$.

363



364

365 **Figure 7: Correlation between the conversion factor K_c/nPSII and the expression of NPQ_{NSV} .**
 366 NPQ_{NSV} was derived as F_o'/F_v' (McKew et al., 2013), for each step of the FRRF light curve at
 367 each TP. Values of K_c/nPSII corresponding to the same light intensities were derived by
 368 extrapolation along the carbon fixation and ETR_{RCII} based PvsE curves.